INVESTIGATION OF RHEOLOGICAL AND NANO-RHEOLOGICAL PROPERTIES OF ASPHALT BINDERS

A Thesis

by

POOYAN KABIR

Submitted to the Office of Graduate and Professional Studies of
Texas A&M University
in partial fulfillment of the requirements for the degree of

MASTER OF SCIENCE

Chair of Committee,	Maryam S. Sakhaeifar
Committee Members,	Dallas N. Little
	Charles J. Glover
Interim Head of Department,	Robin Autenrieth

August 2014

Major Subject: Civil Engineering

Copyright 2014 Pooyan Kabir

ABSTRACT

The study of asphalt emulsion needs a fundamental knowledge of the physical and chemical properties of emulsion. This work investigate different evaporative residue recovery methods as they relate not only to macro scale properties but also to the asphalt microstructure and nano-rheology. Furthermore, this study demonstrates the application of dynamic shear rheometer for macro scale and the application of atomic force microscopy imaging for nano-scale. Extraction of nano-scale engineering properties, i.e. dissipated energy, elastic modulus, adhesion force provide information for prediction of performance related characteristics. This work implements the framework of mechanics by investigating two different solution, elastic and viscoelastic as they relate not only to macro-scale properties of the binder but also to the binder microstructure. It was revealed that different evaporative recovery methods induces substantial microstructural changes in residual binder, i.e. phase distribution, phase percentage, phase structure. It has also been shown that mechanical behavior of asphalt microstructure correlates with bulk behavior of the binder through experimental measurements and finite element modeling techniques.

The rheological properties of binders are now commonly used in materials specifications and are used as input to the Mechanistic-Empirical Pavement Design Guide (MEPDG). Therefore, an approach of using predictive models to estimate the rheological properties of the bituminous materials accurately would be useful for the pavement design. In this study, a modeling approach is proposed which is based on fundamental viscoelastic

principles. To establish the models, a large data set that was obtained from multiple existing national efforts across the United States was used. The database consists of measured modulus values from mixtures with modified and unmodified binders, and mixtures having various amounts of reclaimed asphalt pavement (RAP). As a result, two predictive models were developed to estimate the binder shear modulus and phase angle given the desired physical and mechanical properties of asphalt mixtures. These models can be used for a wide range of temperatures (covering -10° up to 54.4°C) that are recommended in the American Association of State Highway and Transportation Officials (AASHTO) TP62-03 test protocol. It is believed that the aforementioned findings of this study can lead to enhance the knowledge of rheological properties of binders in RAP mixtures at intermediate and high temperatures without the need to extract binder from mixture.

DEDICATION

This thesis is dedicated to my family for their

Love, Support, and Encouragement

throughout my life

ACKNOWLEDGEMENTS

I would like to express my deep gratitude to my thesis adviser Dr. Maryam S. Sakhaeifar for her support and guidance during the course of my graduate study at Texas A&M. To me, she was not just a thesis adviser; she was a magnificent scientist and a very caring mentor. She willingly gave me hours of her time whenever I needed her or whenever I dropped by her office. Also, I would like to thank my committee members, Dr. Little, and Dr. Glover for their technical and helpful advices.

Thanks also go to my friends and colleagues and the department faculty and staff for making my time at Texas A&M University a great experience.

Finally, I thank my parents Eng. Kabir and Dr. Lotfi, as well as my brother Poorya, for their understanding and support during my graduate study in the United States. I have been blessed by a wonderful family who surrounded me with love and care from my first day of life. To them I say thank you.

TABLE OF CONTENTS

Page

ABSTRACT ii

DEDICATION iv

ACKNOWLEDGEMENTS v

TABLE OF CONTENTS vi

LIST OF FIGURES viii

LIST OF TABLES x

1. INTRODUCTION 1

1.1 Overview 1
1.2 Problem Statement 4
1.3 Research Objectives 5
1.4 Thesis Outline 6

2. INVESTIGATING THE EVOLUTION OF EMULSIFIED BINDER NANO-RHEOLOGY USING ATOMIC FORCE MICROSCOPY 8

2.1 Introduction 8
2.2 Materials and Experimental Plan 11
2.2.1 Sample Preparation 12
2.2.2 Equipment 12
2.3 Test Methods 13
2.3.1 Multiple Stress Creep and Recovery (MSCR) and Sweep Strain Results 14
2.3.2 Atomic Force Microscopy Results 18
2.3.3 Fourier Transform Infrared Results 24
2.4 Simulation of Microstructure 25
2.4.1 Simulation Procedure 26
2.4.2 Simulation Results 28
2.5 Conclusions and Recommendations 30

3. NANO-INDENTATION OF MICROSTRUCTURE OF BITUMEN 32

3.1 Introduction 32
3.2 Objective 35
3.3 Materials and Experimental Plan 35

3.3.1 Sample Preparation....36
3.3.2 Equipment....36
3.4 Analytical Solution....37
3.5 Test Results....44
3.6 Conclusions and Recommendations....51

4. AN ANALYTICAL APPROACH TO ESTIMATE THE RHEOLOGICAL PROPERTIES OF ASPHALT BINDERS USING MIXTURE PROPERTIES....53

4.1 Introduction....53
4.2 Objective....57
4.3 Theoretical Formulation....57
4.4 Database Used in This Study....62
4.5 Modeling Approach....65
4.6 Performance of New Predictive Models....67
4.7 Performance of Existing Predictive Models (Hirsch Model)....71
4.8 Summary and Recommendations for Future Study....76

5. CONCLUSION AND RECOMMENDATIONS FOR FUTURE RESEARCH....78

5.1 Conclusions....79
5.2 Future Work....82

REFERENCES....85

LIST OF FIGURES

Page

Figure 1 J_{nr} at Different Aging Conditions for MSCR Testing at 60°C Testing Temperature for (a) 100Pa and (b) 3,200Pa Stress Levels. 15

Figure 2 Average Percent Recovery at Different Aging Conditions for MSCR at 60°C Testing Temperature for (a) 100Pa and (b) 3,200Pa Stress Levels. 16

Figure 3 Failure Strain as Function of Aging for Sweep Strain at 25°C 17

Figure 4 Resistance to Permanent Deformation Criteria as Function of Aging 18

Figure 5 Adhesion Image of Control Binder (Color Scale Shows Relative Differences in Phases Based on Tip Adhesion during Scanning) 19

Figure 6 Topography Images (25μm×25 μm) of Control Binder at a(i) Original, a(ii) PAV, Residue Using Procedure A (after 48 hrs Recovery: 24 hrs @ 25ºC and 24 hrs @ 60ºC) at b(i) Original, b(ii) PAV, and Residue Using Procedure B (after 6 hrs Recovery @ 60ºC) at c(i) Original and c(ii) PAV Aging Conditions. 20

Figure 7 Results of Force-Distance Curves from AFM Testing 22

Figure 8 FTIR Spectra for Different Recovery Methods 25

Figure 9 ABAQUS Parts Input with AutoCAD for Control Binder at (a), Using Procedure B at (b), and Residue Using Procedure A at (c) for Original Condition 27

Figure 10 Tensile Loading Applied to Microstructure of the Control Binder 28

Figure 11 Simulated Maximum Principle Strain for Control Binder at (a), Using Procedure B at (b), and Residue Using Procedure A for Original Condition 29

Figure 12 A Typical Force versus Indentation Depth Curve from an Experimental Indentation Test 34

Figure 13 A Schematic Representation of Load versus Indenter Displacement 37

Figure 14 A Schematic Representation of a Section through an Indentation 39

Figure 15 A Schematic Representation of a Loading, Holding, and Unloading through Indentation 40

Figure 16 Linear Viscoelastic Models used for Formulating the Indentation: (a) Maxwell Model; (b) Kelvin-Voigt Model; (c) Kelvin-Voigt- Maxwell Model 41

Figure 17 A Schematic Indentation on a Sample with Conical Indenter 44

Figure 18 Adhesion Images (25μm×25 μm) of Control Binder at (a), Using Procedure B (after 6 hrs Recovery @ 60ºC) at (b), and Residue Using Procedure A (after 48 hrs Recovery: 24 hrs @ 25ºC and 24 hrs @ 60ºC) at (c) for Original Condition 46

Figure 19 Adhesion Image of Control Binder Processed by ImageJ 47

Figure 20 Back-Analysis of the Holding Response h(t) of a Conical Indentation Test on Phase 3 of Control Binder for Kelvin-Voigt Viscoelastic Model 50

Figure 21 The |*G**| Model Predictions Versus Measured Values Using (a) 90% NCSU, (b) 10% NCSU , (c) Witczak, and (d) AMPT Databases in Logarithmic Scale. 68

Figure 22 The Phase Angle Model Predictions Versus Measured Values Using (a) 90% NCSU, (b) 10% NCSU, (c) Witczak, and (d) AMPT Databases in Arithmetic Scale. 69

Figure 23 Predicted and Measured (I) Shear Modulus and (II) Phase Angle Mastercurves for (a) PG 64-28 from AMPT, PG 64-22, and (b), RAP in Mixtures 71

Figure 24 The Hirsch model |*G**| Predictions Versus Measured Values for (a) 90% of NCSU, (b) 10% of NCSU, (c) Witczak, and (d) AMPT Databases in Logarithmic Scale. 74

Figure 25 The Hirsch Model Phase Angle Predictions Versus Measured Values for (a) 90% of NCSU, (b) 10% of NCSU, (c) Witczak, and (d) APMT Databases in Arithmetic Scale. 75

LIST OF TABLES

Page

Table 1 Effect of Molecular Polarity on the Viscosity of Asphalt Fractions of the Same Molecular Weight 10

Table 2 Summary of Interpreted Information from AFM Test 24

Table 3 Summary of Threshold for Different Phases 47

Table 4 Summary of Percentage Area of Different Phases 48

Table 5 Viscoelastic properties Extracted from the Indentation Holding Phase Using Kelvin-Voigt Viscoelastic Model for Original Aging Condition 51

Table 6 Summary of $|E^*|$ Data Available in NCSU Calibration Mixture Database 64

Table 7 Description of the Developed Models and their Statistics 76

1. INTRODUCTION

1.1 Overview

The approximately 4 million mile-long national road network of the United States provides the basis for economic prosperity. The demands of and reliance upon the American pavement system for mobility and commerce have increased substantially over the past few decades. The total length of the roads in the U.S., paved with either asphalt or concrete is about 2.3 million miles, out of which approximately 96% have hot mix asphalt (HMA) [1]. Asphalt concrete is the desirable paving material due to its availability in nature, initial cost, and its constructability in different volumes and different applications. A recent report from the US Department of Transportation indicates that between 1990 and 2012, truck volumes increased more than 35 % on American highways. Over the same period of time, US highway capacity increased by 6%. The prediction for the next 20 years shows an increase of 50 percent while capacity is expected to continue growing at a much slower rate than volume[2]. HMA mixtures in these pavements are subjected to a wide range of loads, temperatures, and oxidation. The response to these loading conditions is complex and involves the elastic, viscoelastic, and plastic characteristics of the material used in pavements. The response of the pavement structure is dependent on the stiffness of the HMA mix used. In the early 1950 s, Van der Poel of the Shell Oil Company introduced the term “stiffness” (or stiffness modulus)[3]. Generally, the stiffness of a HMA mix is known as a modulus that is dependent upon the loading time and temperature of the mix. The stiffness of a HMA mix is a modulus that is

dependent upon the rheological properties of binder and the gradation and volumetric of the mix.

The importance of rheological properties of bituminous materials has grown in the US since the early 1990 s following the Strategic Highway Research Program (SHRP). These rheological properties are now commonly implemented in materials specifications and are used as input to the Mechanistic-Empirical Pavement Design Guide (MEPDG). The need to know rheological characteristics of bituminous materials becomes more important when combined with the need to characterize the rheological properties of extracted binder from existing asphalt pavement. This need has increased with the use of more reclaimed asphalt pavement (RAP) into HMA to conserve resources and reduce costs. Therefore, the use of simple methods like mathematical modeling to obtain the desired rheological properties would be an advantage. Some researchers [4, 5] evaluated the possibility of back-calculating the physical properties of the blended binders at critical temperatures from the mixture stiffness. In these cases, the critical temperatures from the mixture stiffness will be used to specify the amount of RAP allowed in the mixture.

Due to aforementioned factors, the knowledge of predicting the asphalt concrete pavement performance has been evolved throughout years by many different researchers. Asphalt researchers try to investigate and understand the relationship between asphalt chemical composition and asphalt performance in the field. In the last several decades, researchers developed multiple asphalt behavioral models. Also the use more advanced techniques such as continuum mechanics, and finite element methods in conjunction with laboratory testing of mixture and binder has led to predict the performance of asphalt

concrete pavements more accurately. Due to the magnitude of the asphalt concrete pavement network, a minor improvement can have a substantial effect. Also, production of asphalt concrete pavements consist of energy processes such as distillation of petroleum, transport, storage, mixing, and placement of asphalt concrete that consume energy and resources. To improve this situation, new technologies have been introduced to the asphalt industry, including mixtures with larger amounts of RAP products and emulsion binder for cold construction.

In the early part of the 20th century, the use of asphalt emulsion began. Today around 10 percent of paving grade asphalt is used in emulsified form, but the extent of emulsion usages varies widely between countries. The advantages of asphalt emulsion compared to hot asphalt and cut-back binders are related to the low application temperature, easier handling and storage, compatibility with other water based binders like rubber latex and cement, low solvent content, and environmentally friendly solutions. Therefore, different characteristics of bitumen emulsions need to be evaluated in order to predict the field performance. These characteristics can be storage and transport stability, emulsion break time, and rate of cohesion build up, etc. However, another factor that is crucial for the quality of a road surfacing is the characteristics of the binder itself, after the emulsion has broken. For investigation of physical properties of emulsion binders, a recovery method should be used to extract the residue binder. Different recovery methods have been developed to extract the residue binder with as little influence as possible on its properties, which were documented in the AASHTO specifications.

1.2 Problem Statement

Increase in material costs and use of sustainable materials have led many agencies to consider allowing higher percentages of reclaimed asphalt pavement in asphalt mixes. Reclaimed asphalt concrete consists of both aggregate and aged asphalt binder, so incorporating it into asphalt mixture requires accounting for the RAP aggregate and asphalt during the mix design process. While extraction and recovery using solvents is a common method used to obtain the binder to measure the properties of aged bitumen, the effect of solvents on the measured properties of recovered binders has been widely questioned in addition to the safety of the procedure. For prediction of the rheological properties of the existing binder, the binder from RAP mixtures needs to be extracted, tested, and analyzed. During the construction and service life of the roadway, the asphalt binder ages or hardens ,which changes the properties of the binder prior to the material being used as RAP. Therefore, the properties of RAP materials need to be characterized properly to understand their characteristics at the time of construction. Different studies identified in the literature have shown that 100 percent blending of virgin and the RAP binder does not occur. Also, there are some concerns on whether or not blending charts are really the best method for designing high RAP mixtures. Therefore, this research implements the use of dynamic modulus of mixture (|E*|), volumetric, and gradation parameters in a predictive model to back-calculate the shear modulus of binder (|G*|) used in the mixture.

Substantial improvements have occurred over the years to make quality bituminous emulsion productions and to subsequently apply them in the field. Despite

prodigious efforts of asphalt researchers that have led to significantly improved emulsion pavement performance, there is still limited understanding of the complex micromechanical behavior of these emulsions after breaking down. There have been some attempts to perform rheological tests on the asphalt emulsion residue. Also different researchers [6-8] investigated different recovery methods with commercially available devices (macro scale) to show the differences between mechanical properties of these recovery methods. However, the results were questioned because of the recovery procedure used.

While instrumentation exists to perform rheological tests, the stumbling block for the asphalt emulsion industry to implement such a rheological approach is the lack of an acceptable recovery method that would be suitable to all emulsions. Despite these mechanical properties in bulk volume, new methods that will efficiently provide micro structure and small scale mechanical properties are needed. Therefore, this research implements atomic force microscopy technology (AFM) to expand the knowledge of asphalt binder micro -rheology in order to link the observed behavior to of macro scale to chemical composition and microscopic behavior.

1.3 Research Objectives

The first goal of the research was to develop an experimental setup and use modeling techniques to evaluate different behavior of two available residues recovery methods in two different scales in different aging conditions. This part of the study focuses on characterizing emulsion binders by acquiring the experimental data and applying various modeling techniques.

The second goal of this study is to develop new predictive models to determine the rheological properties of asphalt binder. The models use the asphalt mixture dynamic modulus test data, mixture gradation, and volumetric parameters using the time-temperature superposition concept. The models can be used to estimate the dynamic shear modulus ($|G^*|$) and phase angle of a binder with given desired mixture properties for a wide range of needed testing conditions.

The objectives of this study were achieved by performing the following tasks:

- Improve mathematical model for back calculating binder properties.
- Equip optimization methods to minimize the error associated with modeling.
- Validate sample preparation for small scale experiment.
- Identify the most suitable recovery method for asphalt emulsion available in the literature to obtain residue.
- Perform rheological tests on recovered residues and virgin binder at different aging conditions.
- Perform mechanical testing on microstructure of the bitumen.
- Equip modeling techniques to investigate the behavior of different recovery procedures.

1.4 Thesis Outline

This thesis consists of five chapters that are derived from multiple papers or the ones prepared to be published soon. The thesis is organized into five sections as follows:

- Section 1 presents an introduction that consists of a general overview, problem statement, research objectives, and dissertation outline. For each of the following sections a comprehensive literature review is incorporated to demonstrate how this study contribute to the wider body of the research.
- Section 2 presents the evolution of emulsified binder rheology, and nano-rheology using dynamic shear rheometer (DSR), and atomic force microscopy (AFM) respectively. A comprehensive study of the characterization of an emulsion in different length scales was conducted. Also a simulation of microstructure of the binder was conducted and is presented in this chapter.
- Section 3 presents the nano-indentation of the recovered residue binder of an emulsion. Also this section compares the nano-rheological properties of different residue samples obtained using different recovery methods, and compare them with control binder properties.
- Section 4 presents an analytical approach to estimate the rheological properties of asphalt binders using mixture properties within a mathematical framework.
- Section 5 presents the conclusions and recommendations for future research studies.

2. INVESTIGATING THE EVOLUTION OF EMULSIFIED BINDER NANO-RHEOLOGY USING ATOMIC FORCE MICROSCOPY

2.1 Introduction

An increase in the use of emulsion-based surface treatments has generated the motivation and need to better characterize and understand properties of emulsions that impact their constructability and in-service performance [7]. A number of researchers from around the world [9, 10] have reported microstructural properties of neat and modified asphalt binders based on the results of atomic force microscopy (AFM). Some of the microstructural studies have investigated the impact of oxidative aging [9]. One of the challenges in characterizing the emulsion is to establish a widely acceptable residue recovery method. There are concerns about the applicability of procedures regarding their length and the time required. The recovery by distillation, as defined in ASTM D244, has been reported by a number of researchers to be inadequate due to high recovery temperatures and extended recovery time [11]. A recovery method using temperatures more consistent with those experienced in the field is needed to provide a residue representative of the as-built material and maintain the integrity of binder systems. Recently developed residue recovery methods involve recovery of a thin film of emulsion in a forced-draft oven to address the needs of both recovery at more appropriate temperatures and the ability to produce adequate emulsion for testing [11]. The evaluations of the ASTM method conducted by Hanz et al. and by Kadrmas involved

evaluation of emulsion residue rheological properties and comparison with the unaged base binders [6, 12].

A similar study was conducted by Hanz et al. [7], which focused on evaluating rheological properties at various times during the recovery procedure, for unmodified and modified emulsions, commonly used for chip seals. The results show that the properties of emulsion residue do not reflect those of the unaged base binder, and the evaporative recovery method preserves the effects of modification [6]. Residues produced by the method under development by the New Zealand Transport Agency are using standard test methods of penetration, softening point, and torsional recovery on unmodified and polymer-modified emulsions. Results of both methods of characterization indicate that the residue produced has properties significantly different from those of the unaged base binder [13].

An important component of asphalt durability is defined as the resistance of asphalt to the detrimental effects of oxidative age hardening on its performance properties. In asphalt pavements, oxidative age hardening contributes significantly to pavement embrittlement, eventually resulting in excessive pavement cracking. Oxidative hardening is attributed primarily to the introduction of polar, oxygen-containing chemical functionalities on asphalt molecules causing increased molecular interactions. These changes in chemical composition expected to increase asphalt hardening [14]. The four fractions produced by the Corbett separation scheme in the order of their increasing molecular polarity are saturates, naphthene aromatics, polar aromatics, and asphaltenes. The saturates fraction is generally a light straw-colored oil, primarily hydrocarbon in

nature, with little aromaticity and a low heteroatom content except for sulfur. Corbett [15] described the effects on physical properties of the four generic fractions separated by his procedure as follows: the asphaltenes function as thickeners; fluidity is imparted by the *saturates* and naphthene aromatics fractions, which plasticize the polar aromatics and asphaltenes fractions; the polar aromatics fraction imparts ductility to the asphalts; and the *saturates* and naphthene aromatics in combination with the asphaltenes produce complex flow properties in the asphalt. A proper balance in the amounts of the different chemical components is necessary to produce asphalt that is durable and resistant to detrimental physical property changes that result from oxidative aging [14].

Jemison [16] showed the advantages of using the FTIR-ATR method for asphalt analysis with respect to ease of analysis and repeatability. They also showed that the IR spectra of asphalt samples, due to oven or hot-mix aging or due to apparent reaction in solutions, can be measured. The data in Table 1 were abstracted from data obtained by Griffin et al. [17] to illustrate the effects of different types of molecular interactions on viscosity. It represent the viscosity of each of the three fractions at the same true molecular weight. Because the true molecular weights of each fraction are the same, the differences in viscosity result primarily from differences in the type and strength of the molecular interactions.

Table 1 Effect of Molecular Polarity on the Viscosity of Asphalt Fractions of the Same Molecular Weight

Fraction	Molecular Weight	Viscosity, Pa-s, 25ºC
Saturate	500	10
Aromatic	500	1,000
Resin	500	1,000,000

Source: Adapted from data in Griffen et al. [17]

In this study, the impact of aging in terms of its thermal history on the bitumen micro-structure is reported. The goal was to further understand the link between asphalt chemistry and macroscopic performance by investigating the findings obtained from AFM, DSR, and FTIR testing. Therefore, it was focused on evaluating and comparing the need for the 48-hrs versus 6-hrs recovery time specified in ASTM D7497 to identify the cause of different behaviors relative to base binders. Evaluation was conducted at high and intermediate temperatures on emulsion residues and base binders subjected to different aging conditions. It was revealed that certain asphalt chemical parameters have a consistent and measurable effect, as determined by the AFM, on bitumen microstructures. The initial rheological evaluation of emulsion residue indicates that residue properties from two different recovery procedures are different and they exceed those of the unaged base binder. This research provides new and supporting evidence concerning the influence of aging on properties that ultimately govern macroscopic behavior.

2.2 Materials and Experimental Plan

Three are three different types of binders, control binder, residue recovered based on procedure A at 25ºC for 24 hours followed by recovery at 60ºC for 24 hours, and residue recovered through procedure B at 60ºC for 6 hours. The three different samples were prepared and evaluated at three different aging conditions: original, short term aged (rolling thin film oven: RTFO), and long-term aged (pressure aging vessel: PAV). These binders were selected to compare the difference between evaporative techniques at different aging conditions. The selected emulsion was a CSS-1H, which represents a

cationic slow set emulsion, and the base (control) binder is PG64-22. The volumetric percentage of cationic emulsifier is approximately 3.

2.2.1 Sample Preparation

The asphalt binders were aged for short term aging based on the AASHTO T 240 for RTFO test and for long term aging based on AASHTO R28 using the pressure aging vessel . The residues from emulsified binder were obtained using the AASHTO PP 72-11 including both procedure A (48 hours recovery) and procedure B (6 hours recovery), based on the recovery procedure from AASHTO M140 and AASHTO M208, respectively. The microscope slides were cleaned with methanol before preparing the samples for AFM testing. The slide was heated to 160 °C , cooled down by 30°C intervals ,and was kept at ambient temperature to prevent aging and dust absorption. The amount of 0.2-0.3 grams of binders were spread on a 0.5×3 (cm^2) area to prepare the samples.

2.2.2 Equipment

The Bruker Dimension Icon AFM and the data processing unit were used to measure mechanical properties at room temperature (25 °C). All of the images were obtained by using Peak Force Quantitative Nano-Mechanics (PF-QNM) and MPP-12100-10 silicon cantilevers manufactured by Bruker. The calibrated cantilevers used for this study have an average resonant frequency of 150 kHz, a tip radius of 8 nm, and an average tip angle of 18°. The spring constant of the cantilever used for the experiment was calculated by Thermal Tune in Icon AFM (4.9 N/m).

A Tensor 27 Bruker™ Fourier Transform Infrared (FTIR) spectrometer was used to measure the infrared spectra. The Attenuated Total Reflectance (ATR) method was utilized to collect the spectrum as described by Jemison et al [16].

2.3 Test Methods

The test for characterization of rheological properties of binders using different aging and different evaporative techniques were conducted by using the DSR at intermediate and high temperatures. The multiple stress creep and recovery (MSCR) method was selected to evaluate the permanent deformation criteria and the effects of different aging conditions. The test was performed based on the ASTM D7405.The test was conducted by a 25 mm plate and 1mm gap setting. The sample was loaded for 1 second followed by 9 seconds of rest period. Ten creep and recovery cycles were conducted at 100 Pa creep stress level and ten creep and recovery cycles conducted at 3200 Pa creep stress level. The non-recoverable creep compliance (J_{nr}) and percent strain recovery were used to evaluate the binder modification properties. The fatigue resistance of the binders was evaluated by running a sweep strain test at an intermediate temperature, 25°C, by varying the percentage of strain applied to the samples. The test is comprised of evaluating the effects of increasing the strain on asphalt binder stiffness, $|G^*|$, at a constant frequency and temperature. This test was done using 8mm parallel plate and gap setting of 2 mm. The sweep strain tests were conducted at the frequency of 10 rad/s.

2.3.1 Multiple Stress Creep and Recovery (MSCR) and Sweep Strain Results

The standard suggests use of nonrecoverable compliance (J_{nr}) and percent strain recovery to evaluate test results. Polymer modification allows the binder to accumulate less permanent deformation due to delayed elasticity, so a portion of the deformation is recovered after unloading [18]. Use of the J_{nr} quantifies this behavior and allows for evaluation of the impact of modification on performance. Furthermore, percent strain recovery provides a means to detect the presence of a polymer network and evaluate its development as a function of curing time. These behaviors cannot be captured using the current $|G^*|$ and delta testing protocols; therefore the MSCR test has been adopted and used for polymer-modified binders.

The permanent deformation of binders was evaluated using the MSCR test conducted at 60°C using two sample replicates. The non-recoverable creep compliance of each sample was calculated based on ASTM D7405 and the averaged values of two replicates were used for further evaluation. The results presented in Figure 1 demonstrate the non-recoverable creep compliance (*Jnr*) of two residues using different recovery procedures and a base binder at two different stress levels of 100 Pa and 3,200 Pa. It was found that the Jnr for the PAV aged material are identical regardless of the binder type and the adopted recovery procedure.

The Jnr of the control binder and recovered residue using procedure B are close and they both are different from the residue acquired using procedure A at the short-term aging condition. The values of Jnr are different for both recovered residues and control binder at the unaged condition (original). These results indicate that the recovery of the

modified emulsion residues produces an aged material with rheological properties that approach those of the base binder subjected to the PAV aging. The benefit of modified emulsion is also noted by the significant increase in resistance to permanent deformation (lower Jnr) for emulsion relative to that of base binder at unaged and short-term aging conditions.

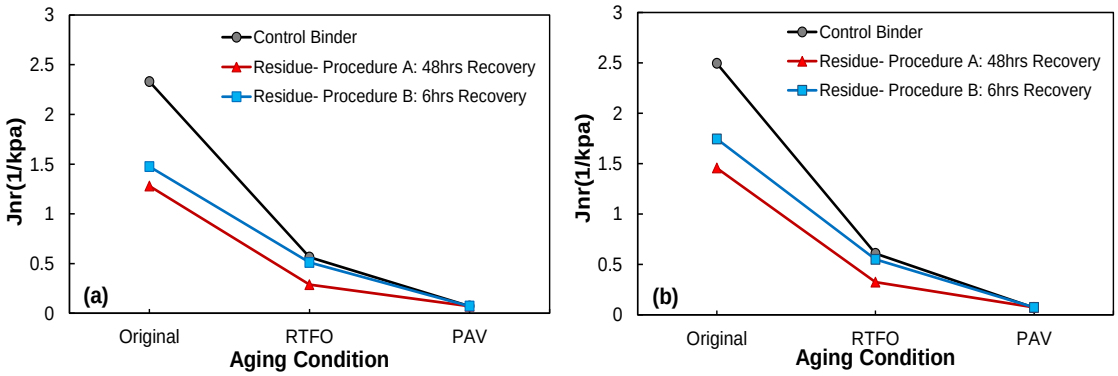

Figure 1 J_{nr} at Different Aging Conditions for MSCR Testing at 60°C Testing Temperature for (a) 100Pa and (b) 3,200Pa Stress Levels.

The average percent strain recovery was used to quantify the development of the polymer network at various aging conditions in the emulsion residues and to compare results to the properties of the base materials. Percent strain recovery is defined as the difference in strain at the end of the creep and recovery cycles. In ASTM D7405, the average percent strain recovery over the 10 cycles of the test at a given stress level is reported [6]. Figure 2 provides results of percent strain recovery evaluation at a 60 ºC testing temperature at stress levels of 100 Pa and 3,200 Pa. The results demonstrate significant differences in the effect of recovery procedures and modification versus the

base binder. At these testing conditions, both the control binder and two residues exhibited negligible percent strain recovery. Both recovered residues show higher percent strain recovery that increases with aging time.

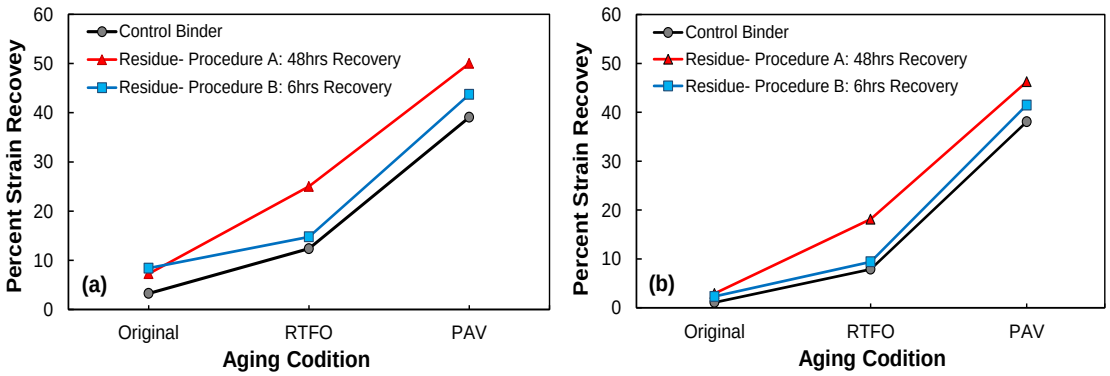

Figure 2 Average Percent Recovery at Different Aging Conditions for MSCR at 60°C Testing Temperature for (a) 100Pa and (b) 3,200Pa Stress Levels.

The failure properties of the control binder and two residues are presented in Figure 3. The results presented in this figure exhibit differing sensitivities to recovery procedures against the control binder. Procedure A exhibits significantly less strain tolerance after 48 hours curing by approximately 8% decrease in failure strain while procedure B leads to 4% decrease in failure strain comparing to the control binder in the original condition. The failure strains of the RTFO-aged binders are very close for both recovery procedures and the base binder and is well below that of original condition which indicates the RTFO material demonstrate less strain tolerance. The PAV-aged residues demonstrate more strain tolerance comparing to the control binder at the same condition. The deviation of behavior of residues from the control binder at different aging conditions

indicate that in regard to strain tolerance, factors other than oxidative aging are affecting the performance of the emulsion residue.

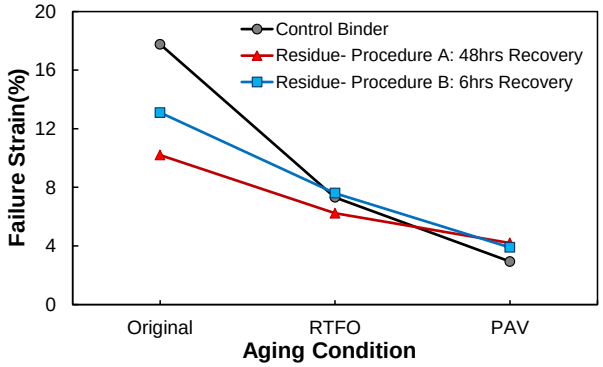

Figure 3 Failure Strain as Function of Aging for Sweep Strain at 25°C

Figure 4 provides the $|G^*|/\sin\delta$ values at different aging conditions. The results for the oven recovered emulsified binder for 48 hours indicate that the curing conditions produces levels of oxidative aging that are different from the other recovered binder for 6 hours and control binder. The largest increase in $|G^*|/\sin\delta$ was observed in RTFO aging condition for the residue recovered for 48 hours. From these results, the properties of the emulsion residues subjected to the ASTM recovery method reflect the effect of latex modification and aging.

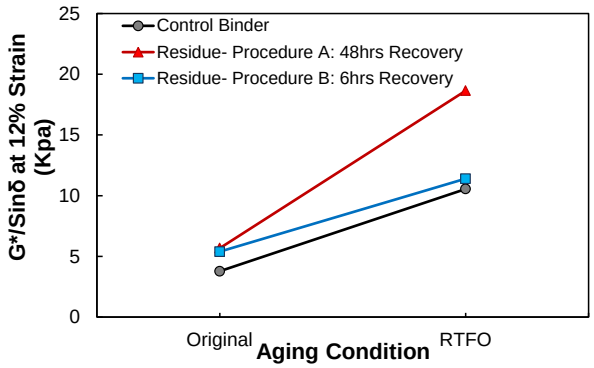

Figure 4 Resistance to Permanent Deformation Criteria as Function of Aging

2.3.2 Atomic Force Microscopy Results

Asphalt chemical parameters have a measurable effect on the asphalt microstructure that can be observed with AFM. Interesting findings can be derived through the interaction of the tip with the microstructure of the asphalt sample using the pull-off force curve [19]. Atomic force microscopy was used in this study to image the surface and identify different phases and microstructures on the specimen surface. This was achieved in non-contact mode as the primary imaging mode. In addition, AFM was used in spectroscopy mode (SM) to measure the nano-scale response of asphalt binders aged at different conditions. Therefore, a combination of these two techniques (AFM and SM) was used to map the microstructure of the asphalt binder and estimate microstructure mechanical properties as illustrated in Figure 5 and Figure 6 respectively. Different phases in an asphalt specimen were identified and a force measurement of each of the phases was performed at different aging conditions for control binder and emulsion residues. The tests consisted of three force measurements taken in each phase. An illustration of different

asphalt phases and locations of each measurement is shown in Figure 5. A 25 μm×25 μm topography image is presented for each asphalt binder, including identification of individual phases and a profile extraction of the corresponding phase topography.

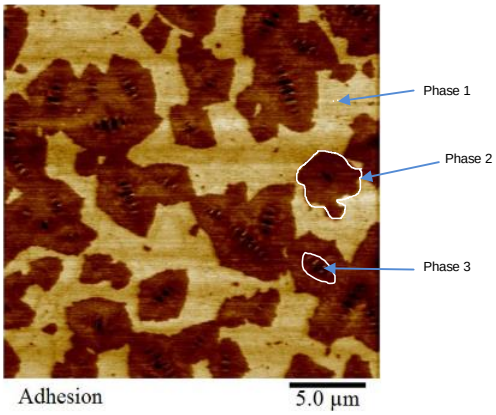

Figure 5 Adhesion Image of Control Binder (Color Scale Shows Relative Differences in Phases Based on Tip Adhesion during Scanning)

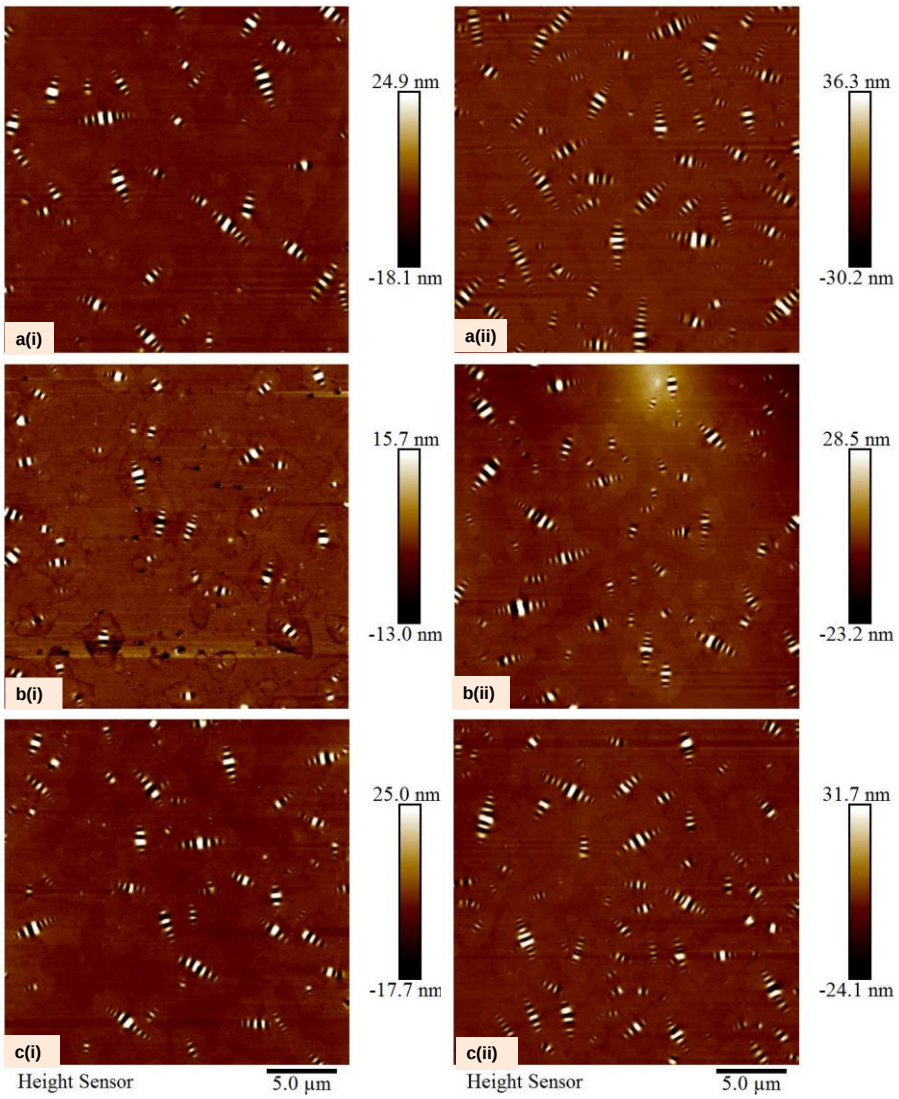

Figure 6 Topography Images (25µm×25 µm) of Control Binder at a(i) Original, a(ii) PAV, Residue Using Procedure A (after 48 hrs Recovery: 24 hrs @ 25ºC and 24 hrs @ 60ºC) at b(i) Original, b(ii) PAV, and Residue Using Procedure B (after 6 hrs Recovery @ 60ºC) at c(i) Original and c(ii) PAV Aging Conditions.

Furthermore, the evaluation of emulsification on asphalt calculated by conducting force distance curves has been shown in Figure 7 and mechanical properties were summarized in Table 2. From the results, it can be concluded that differences are mostly

attributed to physical changes in the asphalt binder and emulsification process. Also hypothesized was that additional source of these differences are potentially oxidation, sample reheating, and residual water. The foaming of the residues during reheating might be another reason. Foaming during reheating indicates the possibility that a thin film was created over the emulsion residue during recovery. In the literature [20], this is referred to as skinning; a similar effect was noted by Takamura in development of the evaporative recovery method when recovery was attempted at high temperatures. This film has a significantly higher stiffness than conventional asphalts do; thus, the presence of the film with the remaining, partially cured, emulsion residue has the potential to increase DSR results.

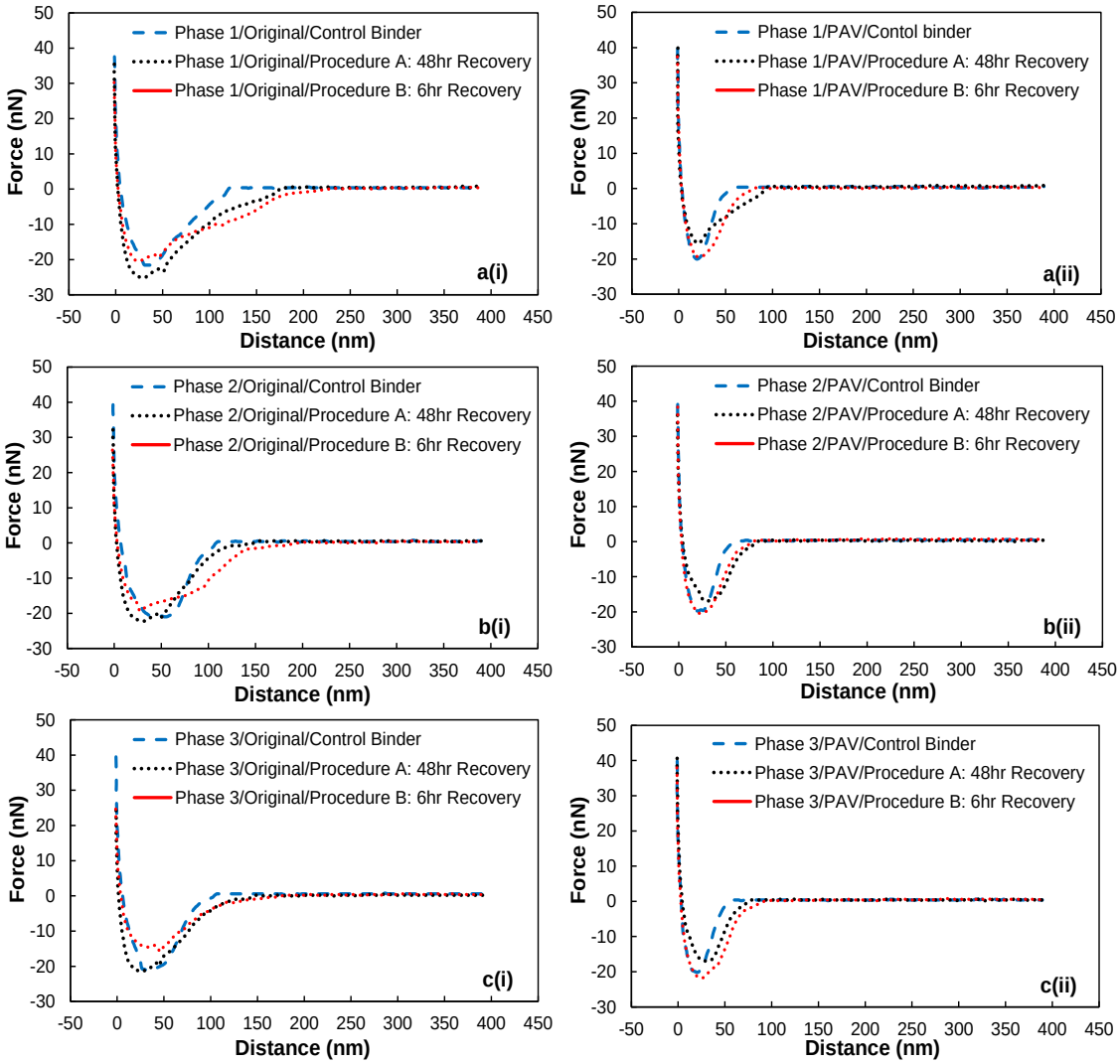

Figure 7 Results of Force-Distance Curves from AFM Testing

The chemistry and micro-rheology of these microstructures within the asphalt binder influence its macroscopic properties, such as stiffness, viscoelasticity, adhesion, fracture and healing. Because the state of component dispersion (component compatibility) of asphalt has a significant effect on asphalt oxidative hardening rate, Peterson [14] suggests that some of the antioxidants may have also reduce oxidative

hardening by acting as a dispersant for the asphaltene-like components in the asphalt that leads to the improvement of component compatibility. Indeed, Dybalski [21] reported that *cationic asphalt additives*, commonly used as asphalt emulsifiers, augment the peptization of the asphaltenes constituent and thus reduce the asphalt hardening rate. According to his findings, of 82 asphalts tested, 81% benefited from the additives, with a minimum of 15% and a maximum of 65% reduction in hardening rate during the RTFO test (ASTM D2872-77). In another study [22], the hardening rate of a recycled pavement mixture during laboratory aging was reduced notably by a high float emulsifying agent used to emulsify the recycling agent before recycling the pavement mixture in the laboratory.

In this study the Young's modulus and energy dissipation of different phases were calculated for the control binder and emulsion residues aged at different conditions. The findings have been summarized in Table 2. The Young's modulus was calculated based on the Sneddon indentation theory by using the spring constant, tip radius, tip half angle and the sample Poisson's ratio. This parameter was used to compare the stiffness of different phases although the response was not purely elastic in this set of tests. The dissipated energy was also calculated based on the area under the force distance curves. As it was expected the dissipated energy decreases in more brittle materials like the control binder and recovered residues in PAV aging conditions compared to the unaged (or original) conditions. An interesting finding is that the dissipated energy was higher for recovered residues compared to the control binder at each aging conditions which indicates the dominant effect of emulsifying process in the residues obtained based on two adopted evaporative recovery procedures.

Table 2 Summary of Interpreted Information from AFM Test

Binder Type	Mechanical Properties	Young 's Modulus (Mpa)		Energy Dissipation (nm×nN)	
	Aging Condition	Original	PAV	Original	PAV
Control Binder	Phase 1	200	610	1354	553
	Phase 2	150	585	1339	623
	Phase 3	185	840	1137	600
Residue-Procedure **A** (48 hrs Recovery)	Phase 1	533	625	2138	705
	Phase 2	466	526	1583	754
	Phase 3	476	716	1482	677
Residue-Procedure **B** (6 hrs Recovery)	Phase 1	350	888	2061	786
	Phase 2	200	643	1730	839
	Phase 3	250	775	1110	1010

2.3.3 Fourier Transform Infrared Results

Asphalt chemical parameters have a measurable effect on the aging of asphalt that can be observed with FTIR to reveal the chemical difference. The area under the peak between 1650 and 1820 wavenumber (cm^{-1}) was measured to determine if the asphalt was oxidizing during the curing processes. The carbonyl area has been shown to be a good measure of oxidation [23]. The Carbonyl areas are 0.69, 0.79, and 0.81 for control binder, 6 hours recovery, and 48 hours recovery respectively. FTIR spectrum showed that longer process ages the binder more than the shorter recovery method and also no trace of water was founded in the specimens tested. The difference in IR spectrum (Figure 8) can be related to recovery process and the emulsification process.

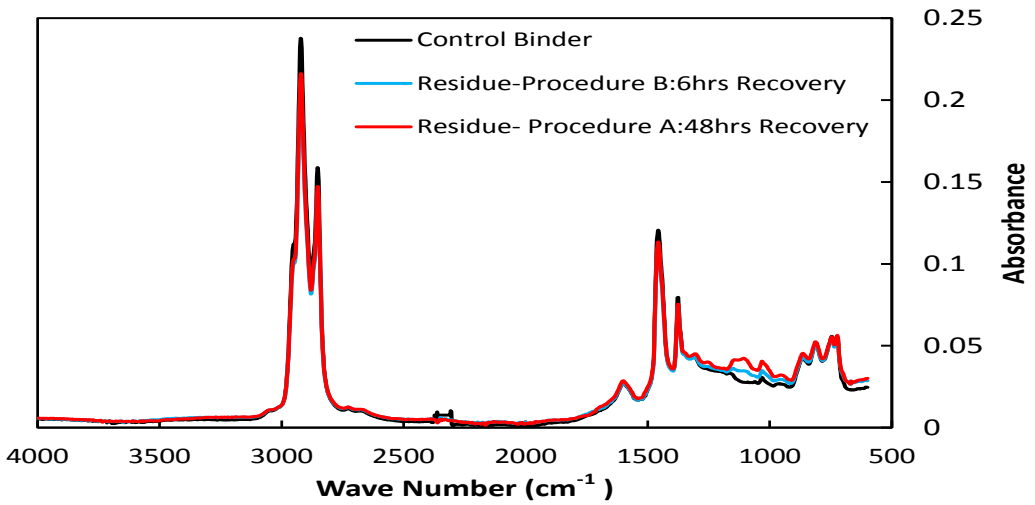

Figure 8 FTIR Spectra for Different Recovery Methods

2.4 Simulation of Microstructure

The microstructure of binder was investigated by different researchers over the last 15 years. The atomic force microscopy (AFM) techniques have been employed to bituminous materials. Loeber et al. [24, 25] have deliberated a comprehensive investigation of bitumen microstructure using AFM by using the heat-casting method to preserve the properties of bitumen. Their investigations revealed rippled structure with micrometer length and nano meter heights which they named bee structure.

Pauli et al.[26] investigated the relation between the amount of asphaltenes and the bee microstructure. The investigation was performed by AFM using both friction- force and tapping mode. Also they doped bitumen with asphaltenes and observed an increase in the density of bee microstructure. Grover et al. [27] investigated the chemical composition of asphalt on micro-rheology of the bitumen with chemical force microscopy and using atomic force microscopy. They doped asphaltenes, napthenic aromatic, resin, and saturate

into two different control binder and investigated the change in different phases. The chemical microscopy reveals the polar behavior of bee structuring and shows that saturates content of asphalt is the primary contributing factor causing bee structuring of non-aged asphalts.

Masson et al. [28] investigated the microstructure of the bitumen by using 12 different types of Strategic Highway Research Program (SHRP) bitumen. In this study they prepared the samples by heat casting method and used phase detection microscopy (PDM). Four detected phases were defined as catanaphase (bee shaped), periphase (casing of catanaphase), paraphrase (solvent regions) and salphase (high phase contrast spots), which were similar to those reported by Jäger et al. [29]. The authors also reported different microstructure of the same bitumen samples prepared by heat casting and solvent casting. Also they presented that not all the bitumen phases contracted equally at low temperatures (-10°C to -30°C). This different contraction could be related to the existence of domains for different phases with different glass transition temperatures.

2.4.1 Simulation Procedure

The adhesion images that were obtained from AFM imaging used for constructing the sketch of phases for ABAQUS as shown in Figure 9. The sketch was built in AutoCAD software and imported to ABAQUS model. The sketch were used to construct different parts in the finite element model, also helped with assembling different part to the model. The material properties were conducted by indentation test. The mechanical properties of phases were used as an input for simulating the behavior of these microstructures. Typical

Poisson's ratio for asphaltic materials can range between 0.1 to 0.5 [30]. In this research study the Poisson ratio for different phases were assumed to be constant and value of 0.3.

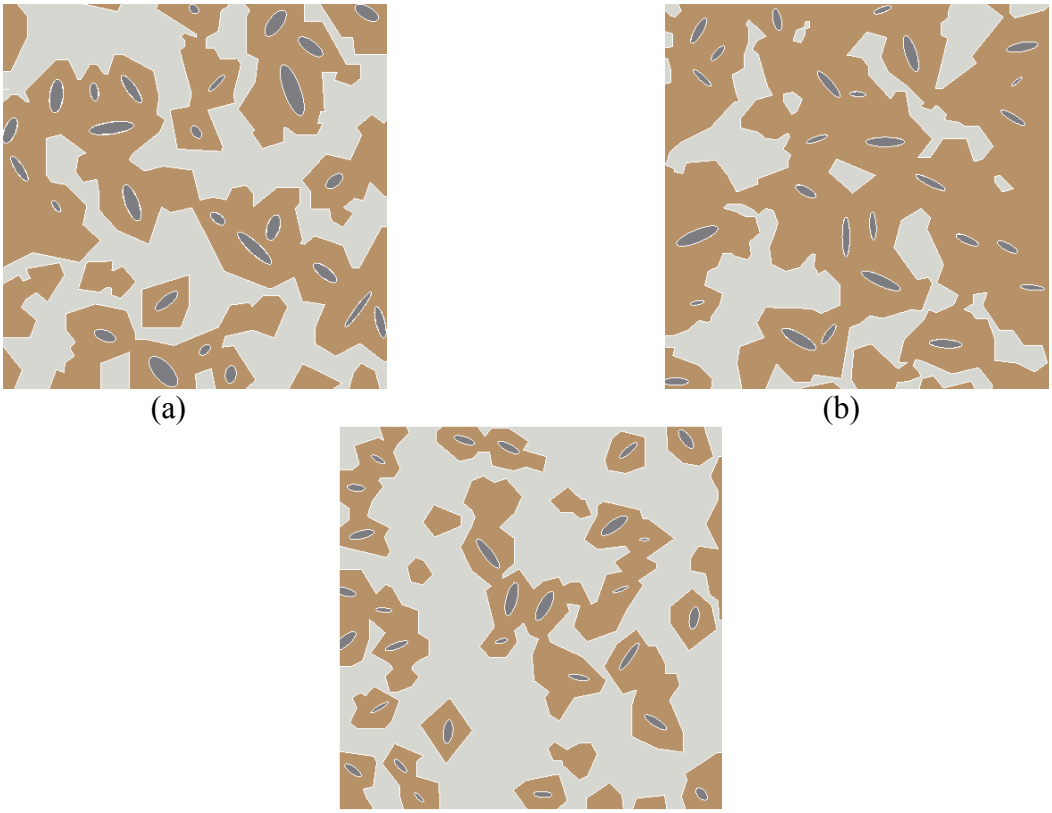

(a) (b) (c)

Figure 9 ABAQUS Parts Input with AutoCAD for Control Binder at (a), Using Procedure B at (b), and Residue Using Procedure A at (c) for Original Condition

For simulation of the microstructure, a tensile static load was applied on both side of the microstructure to investigate the strain tolerance of the microstructure under tension. ABAQUS has not built-in system of units. All input data must be specified in consistent units. For this simulation a consistent set of units were used to investigate the behavior of

the microstructure. A target global element size of 0.1 was used for seed input in the simulations. For simulating the microstructure the element type of 3D stress with quadratic geometric order and reduced integration were used, which makes a C3D20R element type.

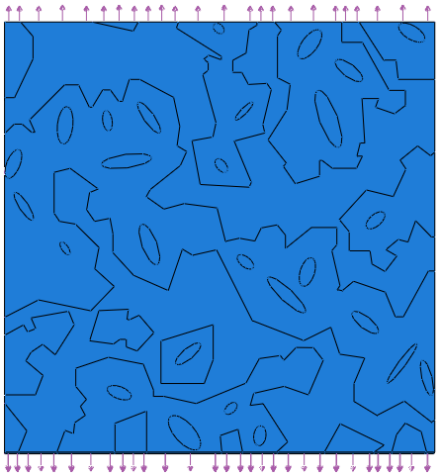

Figure 10 Tensile Loading Applied to Microstructure of the Control Binder

The microstructure of the binder was investigated by applying a tensile loading on both side of the domain as shown in Figure 10. A constant stress of 9 Mpa (N/mm^2) was applied for each microstructure. The load was held constant for all of the microstructures to capture the response under the same loading condition.

2.4.2 Simulation Results

The ABAQUS models were constructed for control binder and residue-recovered binders. The material properties, boundary conditions, and meshing were defined before running the models. The maximum principle strain of control binder, and residue-recovered binders were shown in Figure 10. Further investigation of the simulated

microstructure shown that the highest strain varies for control binder, and residue-recovered binders. All of the microstructures undergoes deformation under the tensile loading but with different maximum strain. The highest strain for control binder, 6hrs recovery, and 48hrs recovery were 0.0866, 0.0833, and 0.0256 respectively.

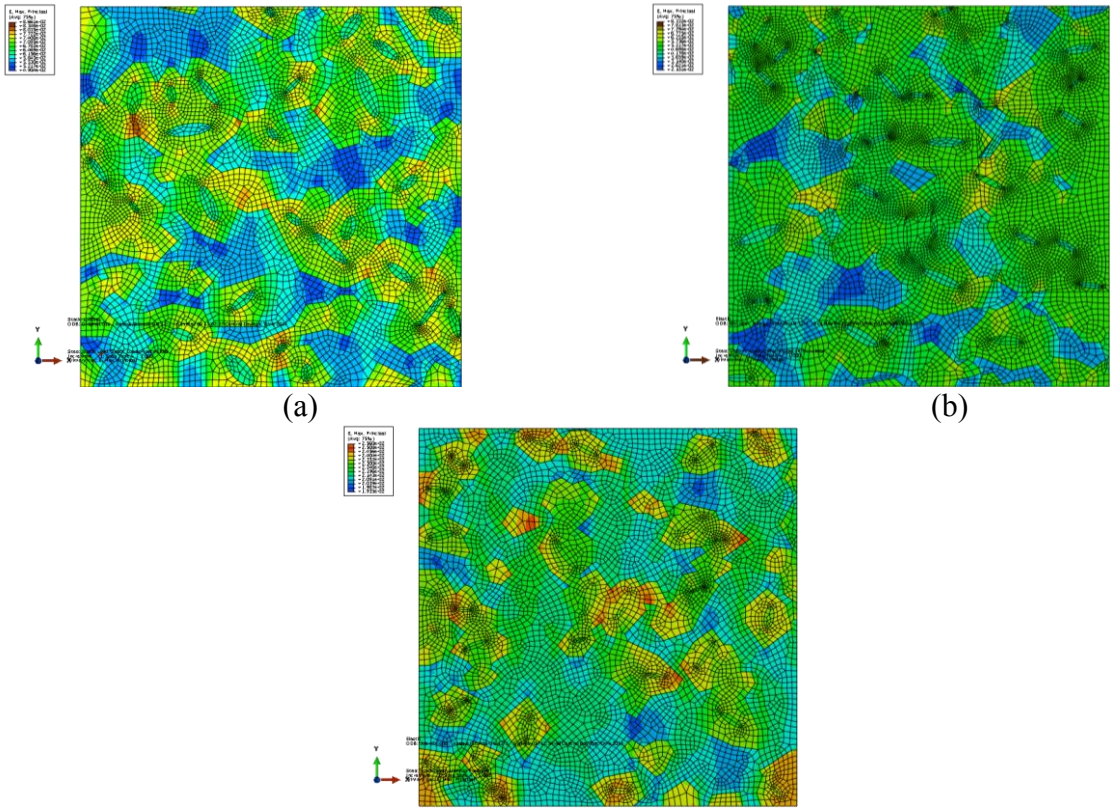

(a) (b)

(c)

Figure 11 Simulated Maximum Principle Strain for Control Binder at (a), Using Procedure B at (b), and Residue Using Procedure A for Original Condition

The highest strain location might be the place for damage and start of degradation of the material. The interesting finding in this study is that the highest strain occurred in

phase 2, bee structuring, for all of the binders (Figure 11). These finding needs a further investigation of hardness of each phase to indicate were the crack initiate and grow.

2.5 Conclusions and Recommendations

The objective of this study was to semi quantitatively characterize the micro-rheology and rheology of a control binder and emulsion residues obtained through different evaporative recovery procedures by using AFM, DSR, and FTIR testing. Based on the results obtained from the study the effects of long-term aging impact not only the material behavior of these microstructures, but also the distribution of each asphalt microstructure. The long-term aging clearly induces microstructural changes in asphalt. The form and extent of these changes, however, were different for control asphalt versus emulsion residues. It is hypothesized that the remaining differences in rheological response as revealed through the evaluations of strain tolerance and percent strain recovery can be related to effects of emulsifier chemistry or different recovery methods. The strain sweep and MSCR produce results that are able to discriminate between recovery procedures and quantify the change in critical properties, as a function of aging time. It was observed that the properties of the emulsion residue do not correspond to those of the unaged base binder. Results support the idea that residue recovered binders be considered as rolling thin-film oven-aged or partially-aged material rather than unaged material. The theme of this research effort was to determine if these differences are due to oxidative aging, remaining moisture, chemistry of the emulsifier, or a combination of these factors.

The findings of this study help the concerns that have been expressed about the length of long evaporative recovery procedure and the possibility for reducing the time

required. Further research is needed to understand the level of aging that occurs in the field relative to the aged state of the residue produced by the recovery method, to quantify the differences in performance between various emulsions and to correlate laboratory performance with actual field performance. The apparent relationships between component ratios and property changes on oxidative aging, as determined by the relationships of the generic fractions, are recommended to be acquired to enhance the results of this study to provide valuable insight into the chemical and physicochemical aspects of asphalt oxidative hardening.

From simulations with actual microstructure model, briefly described in the previous sections, it is evident that different recovery methods can harden the material. The initial configuration and stiffness of phases can thereby have an important characteristic of the bitumen that affects the performance of the bitumen in the field and should be determined. Inhomogeneous distribution of phase affects the ability of bitumen to transmit stresses through its media. Having knowledge about the bitumen distributional phases can so contribute to better prediction of stresses in phases media and reduce damage propagation by engineering the properties. Optimizing the bitumen phases to increase the resilience for stress will enhance the performance of the overall pavement. This requires that molecular weight, densities, and hardness of the bitumen phases should be determined.

3. NANO-INDENTATION OF MICROSTRUCTURE OF BITUMEN

3.1 Introduction

The goal of indentation analysis is to link the indentation data to evocative mechanical properties of the indented material. A typical way to summarize the indentation data is to report two quantities, the hardness H, Equation(1), and the indentation modulus M, Equation(2), which are related to the acquired measurements from indentation data.

$$H = \frac{P_{\max}}{A_c} \tag{1}$$

$$S = \left.\frac{dP}{dh}\right|_{h=h_{\max}} = \frac{2}{\sqrt{\pi}} M \sqrt{A_c} \tag{2}$$

Where,

H = hardness,

$P_{\max}$ = maximum indentation force, N

S = initial slope of unloading curve or indentation stiffness, N/m

A_c = projected contact area,m^2.

The hardness is recognized to be related to strength properties of indented material especially metals [31, 32]. The recent investigation to link the unloading slope S and the elasticity properties of the indented material requires depth sensing indentation techniques that provides a continuous P-h curve during loading and unloading [33, 34].Oliver et al. [34] succesfuly investigated the elastic material properties of alluminum, tungsten, quartz,

and sapphire by acquiring load displacement curves.These indentation techniques can be used to link the classical contact mechanic solutions such as Hertz, Boussinesq, Love, and Sneddon [35-38] to indentation modulus and the elasticity properties of the indented material. For example the indentation modulus and elasticity properties of the indented material by a rigid cone be correlated by Equation(3):

$$M = \frac{E}{1-\upsilon^2} \tag{3}$$

Where,

M = indentation modulus, Pa

E = Young modulus, Pa

υ = Poisson's ratio.

Oliver et al. ,and Vandamme et al.[34, 39] recommended that combining accurate indentation data and Equations(1),(2) one can extract intrinsic mechanical properties of materials that can be described by time independent constitutive relations. The indentation analysis becomes more complicated when used with time dependent constitutive relations [39]. This concept has been implemented successfully for the simplified indentation test that consists of a loading, holding, and an unloading phase as shown in Figure 12.

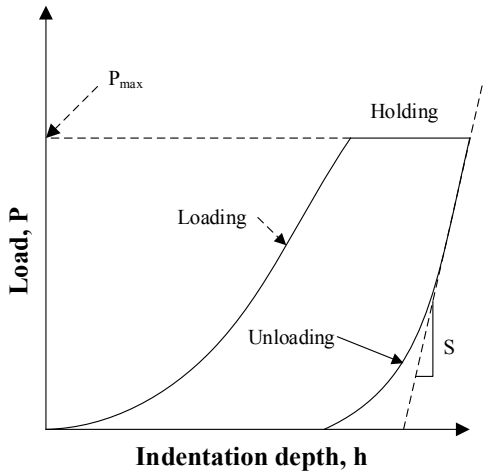

Figure 12 A Typical Force versus Indentation Depth Curve from an Experimental Indentation Test

The load applied on the indenter is increased during the loading phase, then kept constant during the holding phase, and decreased during the unloading phase. The indentation depth increases during the loading, and also holding phase, which leads to an increase in the contact area and a decrease in hardness with time.

Several studies like Domke et al.[40], Raghavan et al. [41], Reynaud et al. [42],and Mondal et al.[43] from various scientific fields, such as cementitious materials, polymer science, and biological sciences, have applied AFM and nano-indention to determine elastic properties of materials. More recently, however, AFM researchers like Davydov et al. [44], Vandamme [45], Moeller et al. [46], and Jonesl et al. [47] have focused on the application of nano-indentation techniques to determine time dependent properties of viscoelastic materials. Jones et al [47] successfully reported the first expressions for viscoelastic uniaxial compliance of calcium silicate hydrate (C-S-H) based on the nano-indentation creep tests of cement paste.

Allen et al. [9] determined the relaxation modulus of asphalt micro-phases to subsequently calculate the composite relaxation modulus values , which provided more information for predicting the asphalt behavior. In their study, the relaxation modulus values were extracted from aged phases of the same asphalt, which provided a relationship between the microstructural changes and changes in composite viscoelastic properties. Jäger et al. [48] identified viscoelastic properties of bitumen and its material phases by means of nano-indentation. They investigated the effects of maximum loading, and loading rate on time dependence parameters of the bitumen by using nonlinear dashpot model. Jäger et al. [48] showed significant variation of model parameters with increase in maximum load, on the other hand a marginal influence of loading rate on model parameters.

3.2 Objective

This study was conducted to investigate the time dependent behavior of each phase and also percentage of each phase in the microstructure of bitumen. Also the indentation creep function was identified for each binder phase to provide the time dependent behavior of each phase and quantify the differences between phases.

3.3 Materials and Experimental Plan

Three different types of binders; control binder, residue recovered based on procedure A (where the binder sample were kept at 25ºC for 24 hours followed by a recovery at 60ºC for 24 hours) , and residue recovered through procedure B (where the samples were kept at 60ºC for 6 hours). These binders were selected to compare the difference of evaporative techniques at original condition. The emulsion used in this study

is “CSS-1H”, which represents a cationic slow set emulsion and the base (control) binder is PG64-22. The volumetric percentage of cationic emulsifier is approximately 3.

3.3.1 Sample Preparation

The residues from emulsified binder were obtained using the ASHTO PP 72-11 including both procedure A (48 hours recovery) and procedure B (6 hours recovery), based on the recovery procedure from AASHTO M140 and AASHTO M208 respectively. The microscope slides were cleaned by methanol before preparing the samples for AFM testing. The slide was heated by 160 °C and then was cooled down by 30°C intervals and then was kept in ambient temperature to prevent aging and dust absorption. The amount of 0.2-0.3 grams of binders were spread on 0.5×3 (cm^2) area to prepare the samples.

3.3.2 Equipment

AFM was developed by Binnig and coworkers in 1986 [49] . Since the improvement of the AFM in the late 1980’s, there have been many technological advances in microscopy techniques, which have made AFM an attractive tool for studying microstructure of materials. Different modes of operation, including contact mode, non-contact mode, tapping mode, and peak force tapping can be used for imaging. Different AFM modes can provide insight into the adhesion, phase difference and mechanical properties of binder at the micro-scale. AFM probes the surface of a sample with a tip while laser on the back of the cantilever reflects the deflection of the tip so the interaction between the sample and the tip are mapped. The geometry of the tip is rotated (symmetric) with the 15-20 μm height, 15° front angle, 25° back angle, and 18° side angle with tip

radius of 8 nm. The geometry of the cantilever is rectangular with 1.85 μm thickness, and back side coating of reflective aluminum.

3.4 Analytical Solution

The problem we consider is the indentation of a rigid cone in a linear viscoelastic material. The indentation test is load controlled and follows a trapezoidal load history. Vandamme et al.[39] successfully used the Oliver-Phar [34] method for contact area estimation to investigate the response of a white cement phase. Oliver-Phar [34] method was used to extract the instantaneous response of the material from unloading curve. In this method the slope, Equation(4), of unloading part of the experiment will be used as shown in Figure 13 as an indication of elastic modulus of indenter and media being indented.

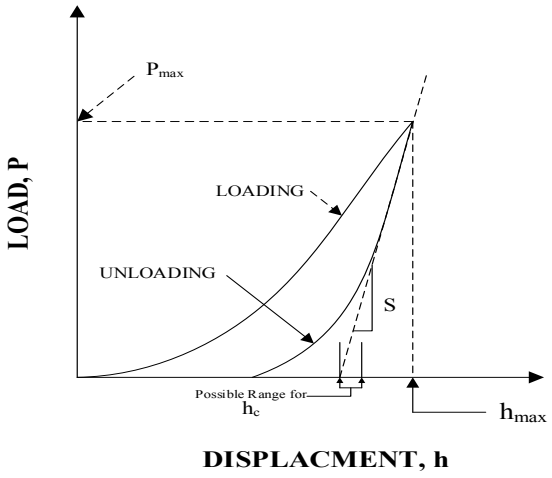

Figure 13 A Schematic Representation of Load versus Indenter Displacement

Equation(4) relates the reduced modulus, E_r, to the contact area, A_c, and the measured stiffness of indented material.

$$S = \frac{2}{\sqrt{\pi}} E_r \sqrt{A_c} \tag{4}$$

Where,

S = initial slope of unloading curve or indentation stiffness, N/m

A_c = projected contact area, m^2

E_r = reduced modulus, Pa.

The relation between reduced modulus, elastic modulus of material, and indenter presented in Equation(5)

$$\frac{1}{E_r} = \frac{\left(1-\upsilon^2\right)}{E} + \frac{\left(1-\upsilon_i^2\right)}{E_i} \tag{5}$$

Where,

E = Young's modulus for specimen, Pa

υ = Poisson's ration for specimen,

E_i = Young's modulus for indenter, Pa

υ_i = Poisson's ration for indenter.

The contact area, A_c, at the peak load was determined by the geometry of indenter and contact depth. It was assumed that the indenter geometry can be described by an area function named $F(h)$ that relates the cross section area to the distance from its tip as described in Equation(6). Also Figure 14 shows the cross section of indentation and identifies the parameters used in the analysis.

$$A_c = F(h_c) \tag{6}$$

Where,

h_c = vertical distance along which contact is made,

$F(h_c)$ = mathematical function to relate depth to contact area.

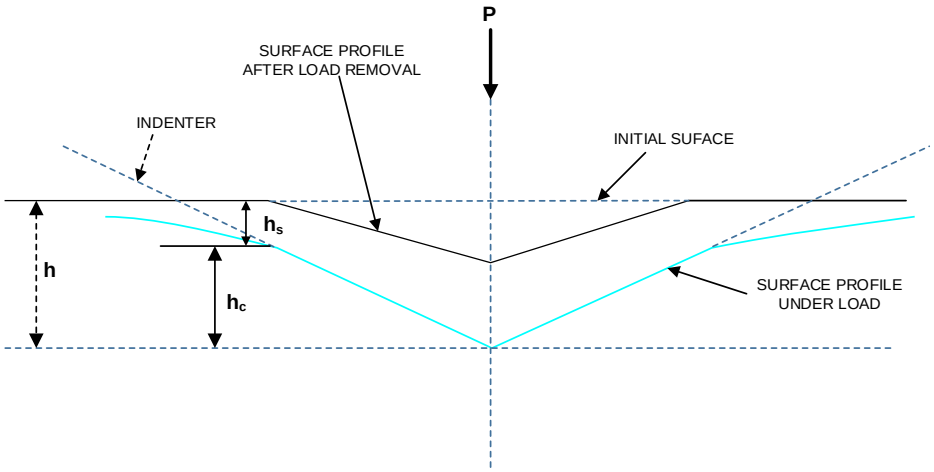

Figure 14 A Schematic Representation of a Section through an Indentation

Equation(7),(8), and (9) was used to calculate h_c and to determine the contact depth from the experimental data.

$$h_c = h_{\max} - h_s \tag{7}$$

$$h_s = \varepsilon \frac{P_{\max}}{S} \tag{8}$$

$$\varepsilon = \frac{2}{\pi}(\pi - 2) \tag{9}$$

where,

h_s = displacement of the surface at the perimeter of the contact, m

P_{max} = maximum load during the indentation, N

ε = geometric constant.

Also, an analytical method developed by Vandamme [39] was used to extract the viscoelastic properties of different phase based on a viscoelastic solution for conical indentation. Vandamme used Sneddon [38] elastic solution with the Radok and Lee functional equation method [50] to solve the indentation of an axisymmetric tip and a viscoelastic body. This method consists of a loading, holding, and an unloading phase, as shown in Figure 15. In the force history data the deflection is measured and used for extracting the material properties.

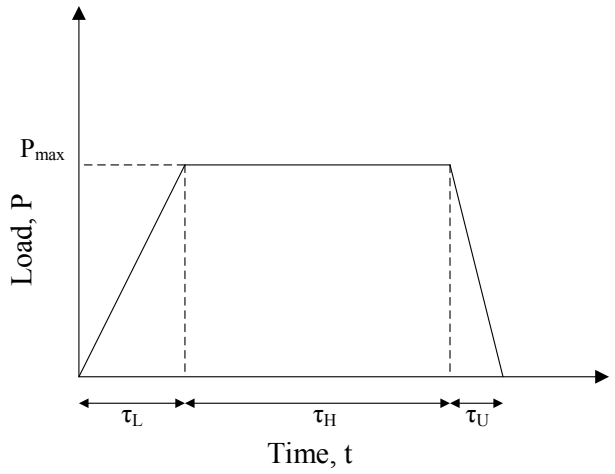

Figure 15 A Schematic Representation of a Loading, Holding, and Unloading through Indentation

The solution developed by Vandamme [39] for a trapezoidal loading and three different linear viscoelastic models are shown schematically in Figure 16.

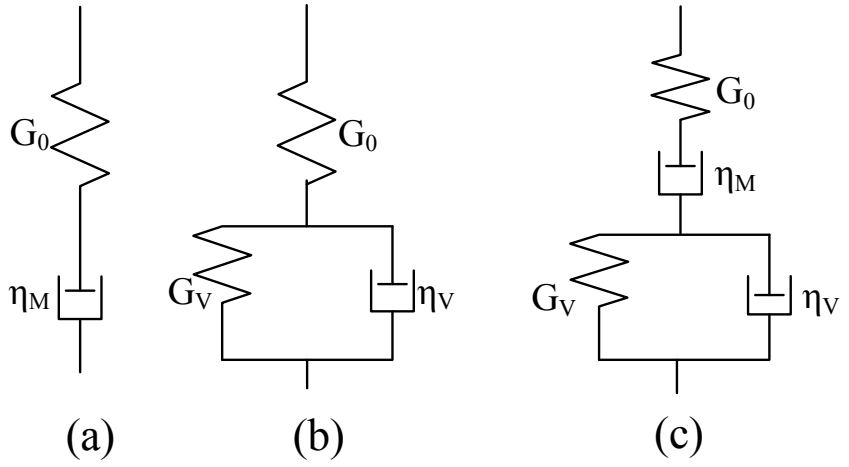

Figure 16 Linear Viscoelastic Models used for Formulating the Indentation: (a) Maxwell Model; (b) Kelvin-Voigt Model; (c) Kelvin-Voigt- Maxwell Model

Vandamme et al. also formulated the problem based on the holding, and loading phase and they were able to solve the solution for each of the loading and holding load steps. Furthermore, they developed a dimensionless solution of the viscoelastic problem as shown in Equation(10):

$$y\ (t) = \frac{2}{\pi}\frac{M_0 h^2(t)}{P_{\max}} 4\tan(\theta) \tag{10}$$

where,

$y\ (t)$ = dimensionless solution,

t = time, seconds

M_0 = indentation depth, Pa

$h\,(t)$ = indentation depth, m

θ = half angle of rigid cone, degree.

The equations that were used for extracting the material properties using Maxwell model were shown in Equation(11), and(12). In Equations (11) through (16) and also for the Maxwell model presented in the following two equations, the terms $y_L(t), y_H(t)$ represent the loading, and holding phase respectively.

$$y_L(t) = \frac{1}{\tau_L}\left(\frac{5-4\upsilon_0}{1-\upsilon_0^{\,2}}t + \frac{M_0}{\eta_M}\frac{t^2}{2} - \left(\frac{1-2\upsilon_0}{1-\upsilon_0^{\,2}}\right)^2 \frac{3\eta_M}{M_0}\left(1-e^{-\frac{E_0}{3\eta_M}t}\right)\right) \tag{11}$$

$$y_H(t) = \frac{5-4\upsilon_0}{1-\upsilon_0^{\,2}} + \frac{M_0}{\eta_M}\left(t-\frac{\tau_L}{2}\right) - \left(\frac{1-2\upsilon_0}{1-\upsilon_0^{\,2}}\right)^2 \frac{3\eta_M}{M_0\tau_L}\left(e^{\frac{E_0\tau_L}{3\eta_M}}-1\right)e^{-\frac{E_0 t}{3\eta_M}} \tag{12}$$

where,

$y\,(t)$ = dimensionless solution,

M_0 = elastic indentation modulus, Pa

υ_0 = Poisson's ration of material indented,

τ_L = time of loading, seconds

η_M = viscosity of the damper, Pa.s .

The solutions for Kelvin-Voigt Model were shown in Equations(13), and(14).

$$y_L(t)=\frac{1}{\tau_L}\left(\left(4+\frac{M_0}{G_V}+(1-2\upsilon_0)^2\frac{M_0}{E_0+3G_V}\right)t-\frac{\eta_V M_0}{{G_V}^2}\left(1-e^{-\frac{G_V}{\eta_V}t}\right)-\frac{3\eta_V M_0(1-2\upsilon_0)^2}{(E_0+3G_V)^2}\left(1-e^{-\frac{E_0+3G_V}{3\eta_V}t}\right)\right) \quad (13)$$

$$y_H(t)=4+\frac{M_0}{G_V}+\frac{M_0(1-2\upsilon_0)^2}{E_0+3G_V}+\frac{\eta_V M_0}{{G_V}^2\tau_L}\left(1-e^{\frac{G_V\tau_L}{\eta_V}}\right)e^{-\frac{G_V t}{\eta_V}}+\frac{3\eta_V M_0(1-2\upsilon_0)^2}{(E_0+3G_V)^2\tau_L}\left(1-e^{\frac{(E_0+3G_V)\tau_L}{3\eta_V}}\right)e^{-\frac{(E_0+3G_V)t}{3\eta_V}} \quad (14)$$

where,

G_V = stiffness of spring in parallel with a dashpot, Pa

η_V = viscosity of dashpot in parallel with a spring, Pa.s.

The solutions for Kelvin-Voigt- Maxwell Model, shown in Equations(15), and(16).

$$y_L(t)=\frac{1}{\tau_L}\left(\frac{5-4\upsilon_0}{1-{\upsilon_0}^2}t+\frac{M_0}{G_V}\left(t-T_2\left(1-e^{-\frac{t}{T_2}}\right)\right)+\frac{M_0t^2}{2\eta_M}-\frac{(1-2\upsilon_0)^2}{(1-{\upsilon_0}^2)\left(\frac{1}{T_1}-\frac{1}{T_3}\right)}\left[\left(\frac{T_3}{T_2}-1\right)\left(1-e^{-\frac{t}{T_3}}\right)+\left(1-\frac{T_1}{T_2}\right)\left(1-e^{-\frac{t}{T_1}}\right)\right]\right) \quad (15)$$

$$y_H(t)=\frac{5-4\upsilon_0}{1-{\upsilon_0}^2}+\frac{M_0}{G_V}-\frac{M_0T_2}{G_V\tau_L}e^{-\frac{t}{T_2}}\left(e^{\frac{\tau_L}{T_2}}-1\right)+\frac{M_0}{\eta_M}\left(t-\frac{\tau_L}{2}\right)-\frac{(1-2\upsilon_0)^2}{\tau_L(1-{\upsilon_0}^2)\left(\frac{1}{T_1}-\frac{1}{T_3}\right)}\times\left[\left(\frac{T_3}{T_2}-1\right)e^{-\frac{t}{T_3}}\left(e^{\frac{\tau_L}{T_3}}-1\right)+\left(1-\frac{T_1}{T_2}\right)e^{-\frac{t}{T_1}}\left(e^{\frac{\tau_L}{T_1}}-1\right)\right] \quad (16)$$

where the time constants T_1, T_2, T_3 are given by Equation (17)

$$\begin{cases} T_1 = \dfrac{6\eta_M\eta_V}{E_0(\eta_V+\eta_M)+3\eta_M G_V+\sqrt{E_0{}^2(\eta_V+\eta_M)^2+6E_0\eta_M G_V(\eta_M-\eta_V)+9\eta_M^2 G_2^V}} \\ T_2 = \dfrac{\eta_V}{G_V} \\ T_3 = \dfrac{6\eta_M\eta_V}{E_0(\eta_V+\eta_M)+3\eta_M G_V-\sqrt{E_0{}^2(\eta_V+\eta_M)^2+6E_0\eta_M G_V(\eta_M-\eta_V)+9\eta_M^2 G_2^V}} \end{cases} \quad (17)$$

where,

η_M = viscosity of damper in series with a spring, Pa.s.

3.5 Test Results

The microstructure of asphalt binders was imaged by atomic force microscopy in peak force mode and the indentation points were picked up in each phase to perform the indentation test. As shown in Figure 17 a conical indenter was used to extract the material properties of different phases of binder.

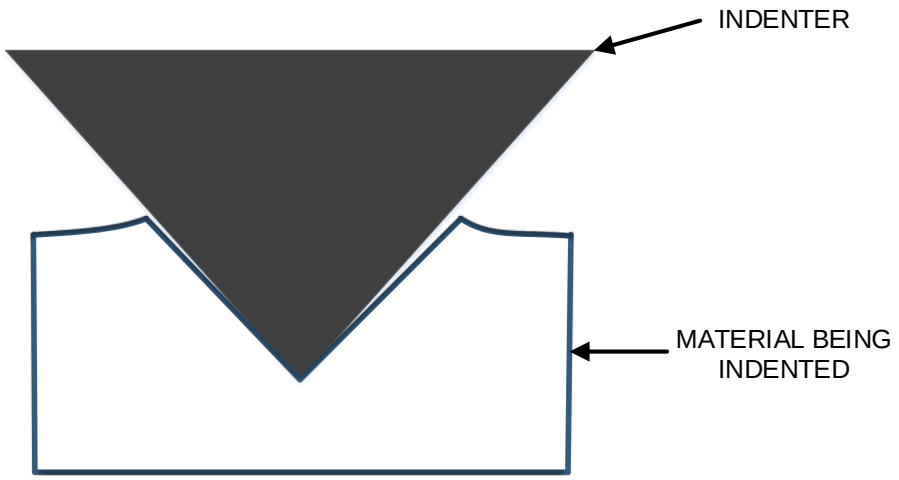

Figure 17 A Schematic Indentation on a Sample with Conical Indenter

The peak force images of different recovery methods and control bindes were obtained by AFM. The adhesion images of control binder, procedure B (6 hours), and procedure A (48 hours) are shown in Figure 18 with three different phases in the adhesion images. For validation of different phases, each phase was indented and different viscoelastic material properties were extracted, which show the difference in mechanical properties of these phases. For this purpose, three different points were chosen to present an average material response for each desired phase. In this study, the percentage of each phase was calculated based on the adhesion image of binders and different aging condition to investigate the evaluation of different phases under AFM. The percentage of different phases were obtained by using ImageJ [51] as an image processing and analysis tool. The adhesion images were converted to 8-bit grayscale images before processing. This conversion will change color images to grayscale images and easier to perform image processing on them.

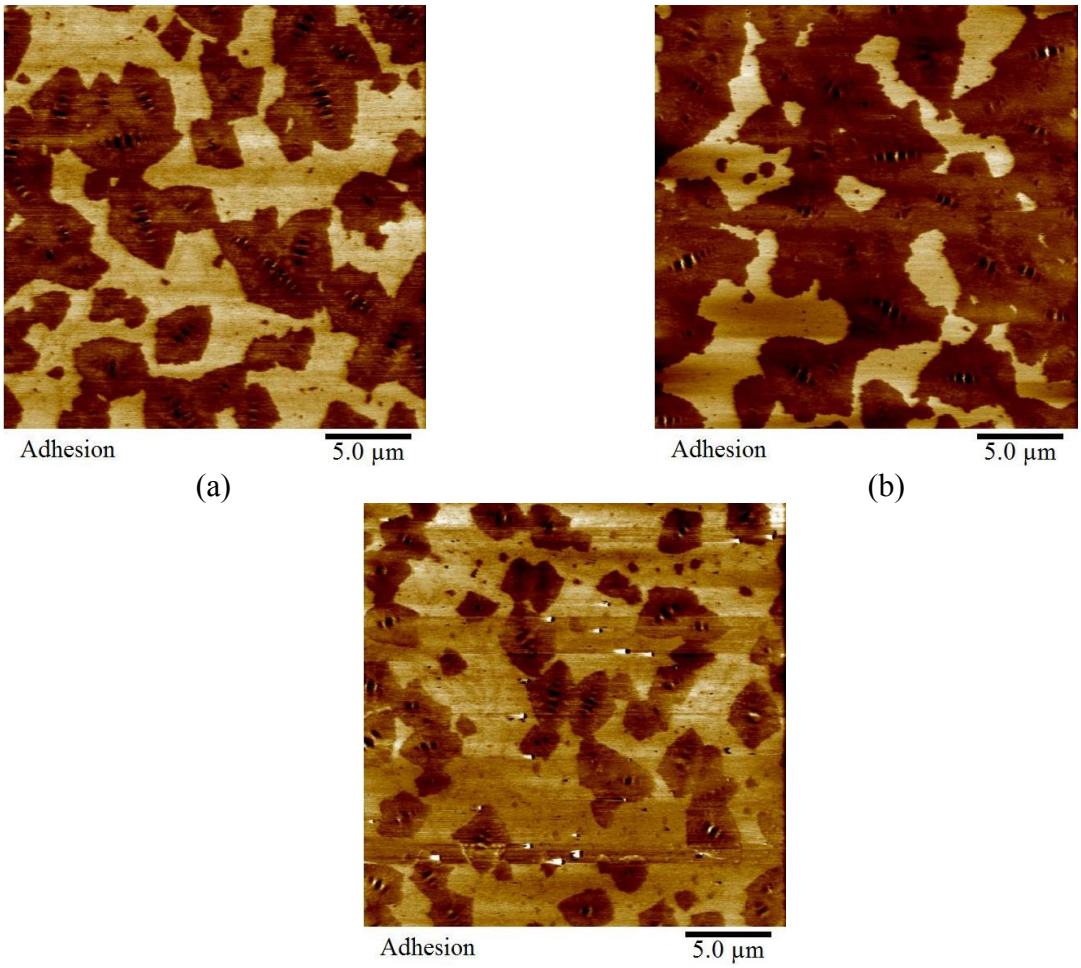

Figure 18 Adhesion Images (25µm×25 µm) of Control Binder at (a), Using Procedure B (after 6 hrs Recovery @ 60ºC) at (b), and Residue Using Procedure A (after 48 hrs Recovery: 24 hrs @ 25ºC and 24 hrs @ 60ºC) at (c) for Original Condition

The 8bit binary representations assume that 0 is black and the maximum value of 255 is white. After conversion to 8bit image the threshold was adjusted to capture different phases. The boundary values for threshold for each phase and image is shown in Table 3.

Table 3 Summary of Threshold for Different Phases

Binder Type	Image Threshold	Range	
	Aging condition	Original	PAV
Control Binder	Phase 1	89-255	89-255
	Phase3	29-255	42-255
Residue-Procedure A (48 hrs Recovery)	Phase 1	73-255	68-255
	Phase3	30-255	28-255
Residue-Procedure B (6hrs Recovery)	Phase 1	60-255	89-255
	Phase3	24-255	35-255

Also, different phases were obtained based on their adhesion images. A representation of the processed image for calculating different phases is shown in Figure 19.

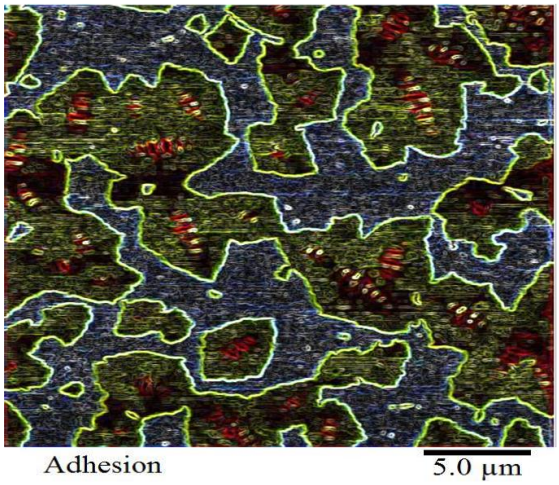

Figure 19 Adhesion Image of Control Binder Processed by ImageJ

The percentage area occupied by each phase was calculated based on Equation(18) , and are summarized in Table 4.

$$\%Area = \frac{A_{i,each\ phase}}{\sum_{i=1}^{3} A_{i,each\ phase}} \times 100 \quad (18)$$

where,

% Area = percentage of area occupied by each phase relative to the total sample area depicted by AFM,

A_i = area of each phase,

i = number of depicted phases.

Table 4 Summary of Percentage Area of Different Phases

Binder Type	Phase Distribution	Percentage Area (%)	
	Aging Condition	Original	PAV
Control Binder	phase 1	40.43	2
	phase 2	49.62	86.87
	phase 3	9.95	11.13
Residue-Procedure **A** (48 hrs Recovery)	phase 1	63	38.71
	phase 2	26.14	45.4
	phase 3	10.86	15.89
Residue-Procedure **B** (6 hrs Recovery)	phase 1	28.5	17.34
	phase 2	64.66	69.76
	phase 3	6.84	12.9

The atomic force microscopy was used to indent the material with a conical indenter. In this experiment the loading, holding, and the unloading time were considered to be 2, 6, and 2 seconds respectively. Furthermore, two calibrations are needed to convert

the voltage information of the AFM to indentation depth, and force. The spring constant value can be found on the specification box of the probe, or measured using thermal tune method [52]. The thermal tune was used to calculate the spring constant of the tip, which was 4.6 N/m. The deflection sensitivity of the tip was calibrated by using a very stiff sample, sapphire, to convert the voltage of the photo diode to deflection. The deflection sensitivity of the tip was measured, which was 62.11 nm/V. This information was then used to convert the experiment data to indentation depth in nanometer, and loading in newton. In addition, the Vandamme [39] solution was used to extract the viscoelastic material behavior. The holding phase of the experiment was used with the corresponding analytical model to get the best fit by minimizing the error.

In this study, Kelvin-Voigt viscoelastic model was used to back-calculate the mechanical responses of all of the phases for control binder, and residue-recovered binders. An example of back-calculation for one of the phases of control binder is shown in Figure 20.

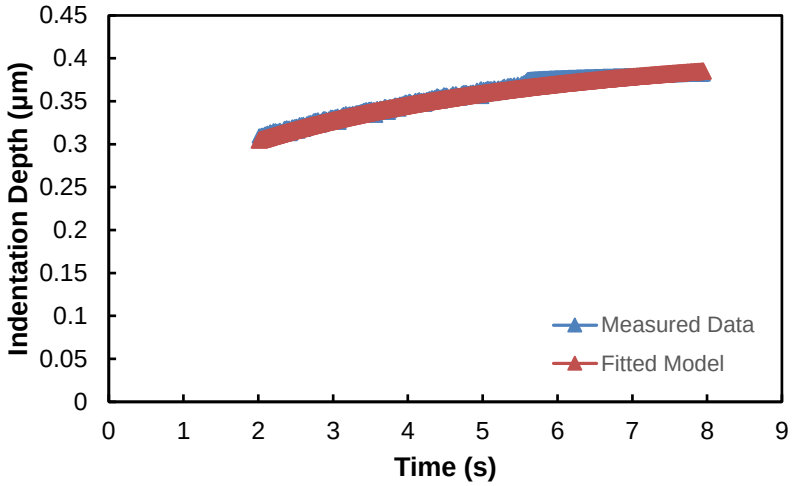

Figure 20 Back-Analysis of the Holding Response h(t) of a Conical Indentation Test on Phase 3 of Control Binder for Kelvin-Voigt Viscoelastic Model

In this study the indentation modulus, M_0, spring stiffness, G_V, and dashpot viscosity,η_v, of different phases were calculated for the control binder and emulsion residues at original aging condition. The findings of this investigation have been summarized in Table 5. As discussed before, the Kelvin-Voigt viscoelastic parameters were calculated based on Vandamme indentation solution by using holding phase of loading history. These parameters were the utilized to compare the elastic response, and viscoelastic response of each depicted phase.

Table 5 Viscoelastic properties Extracted from the Indentation Holding Phase Using Kelvin-Voigt Viscoelastic Model for Original Aging Condition

Binder type	Control Binder			Residue-Procedure A (48hrs Recovery)			Residue-Procedure B (6hrs Recovery)		
Mechanical Properties	Phase 1	Phase 2	Phase 3	Phase 1	Phase 2	Phase 3	Phase 1	Phase 2	Phase 3
M_0 (Mpa)	240	150	200	600	450	500	400	240	280
G_v (Mpa)	45.8	87	40	24	50	24.5	35	72	33.5
η_v (Mpa s)	85	70	200	50	30	67	67	50	120

As it is expected the elastic response of the material was higher in more brittle materials like recovered residue binders. The interesting finding is that the viscosity of the dashpot, and the stiffness of the spring, parallel with dashpot, decrease with increase in evaporation time for residue recovery procedures. This finding in addition to higher dissipated energy for recovered residues compared to the control binder at each aging condition indicates the dominant effect of emulsifying process in the residues obtained based on two adopted evaporative recovery procedures.

3.6 Conclusions and Recommendations

The purpose of this study was to quantitatively characterize the viscoelastic properties of a control binder and emulsion residues obtained through different evaporative recovery procedures by using AFM nano-indentation. Based on the results obtained from the study the effects of recovery methods impact not only the elastic behavior of these microstructures, but also the viscoelastic properties of each asphalt microstructure. The form and extent of these changes, however, were different for control asphalt versus emulsion residues. Different residue recovery methods not only change the

elastic, and viscoelastic properties of each phase, but also the distribution of each asphalt microstructure.

Furthermore, the identification of viscoelastic properties of bitumen and its phases by means of nano-indentation was presented in this study. The back-analysis scheme proposed in Vandamme et al. [39] was used toward implementation of Kelvin-Voigt model for asphalt binder. In order to identify the material parameters of asphalt binder a trapezoidal loading history was applied. The parameters for the Kelvin-Voigt model were determined from the holding period of the indentation test. It was found that the model parameters obtained from indentation testing fit well with experimental data. The findings of this study help the concerns that have been expressed about the length of long evaporative recovery procedure and the possibility for reducing the time required. However, further research is recommended and needed to understand the level of aging that occurs in the field relative to the aged state of the residue produced by the recovery method, to quantify the differen ces in performance between various emulsions and to correlate laboratory performance with actual field performance.

4. AN ANALYTICAL APPROACH TO ESTIMATE THE RHEOLOGICAL PROPERTIES OF ASPHALT BINDERS USING MIXTURE PROPERTIES

4.1 Introduction

The importance of rheological properties of bituminous materials has grown in the US since early 1990's following the Strategic Highway Research Program (SHRP). These properties are the primary parameters described in AASHTO specification M320. These rheological properties are now commonly used in materials specifications and are used as inputs to the Mechanistic-Empirical Pavement Design Guide (MEPDG) [53]. In addition, a large and extensive database including various asphalt mixtures and binders has been collected from test sections around the country. In many of these test sections some of the fundamental material properties have not been determined. An example of this is a large number of the long term pavement performance (LTPP) sections for which neither dynamic shear modulus ($|G^*|$) nor phase angle of binders are reported [54]. Therefore, the use of simple methods to obtain the desired rheological properties would be an advantage and increase the utility of the existing data.

The rheological properties of bituminous materials represent a verification of fundamental mechanical properties. An article in the Society of Rheology mentioned the uncertainty for phase angle measurements that occurs due to the lack of calibration standards [55]. However, adopting the relationships that exist and utilizing these to verify and check the adequacy of the measurements will assist in phase angle measurements [56]. In this regard, Rowe (2009) used the interrelationships between the stiffness and frequency

dependency and successfully verified two different methods for obtaining the phase angle information. The first method was to fit discrete spectra to the complex modulus mastercurve whereas the second one makes use of the log-log relationship between the complex stiffness modulus and frequency and showed how this relates to phase angle [56]. Also, in a study done by Valdes et al. the characterization of different mixtures having up to 60% RAP content was investigated. It was shown how the coarse RAP friction will increase the variability of aged binder content. The results show that the use of a higher percentage of fine RAP friction can decrease variability of aged binder [57].

It is possible to determine some of the rheological properties such as phase angle if only $|G^*|$ or $|E^*|$ data is available by an analysis of the spectra information or from the slope information obtained from the mastercurve. Also, it is possible to determine the phase angle information for both binder and mixture, and the complex shear modulus of the binder given just the complex dynamic modulus of a mixture [56]. Dickersen and Witt (1974) presented a relationship that linked the phase angle of bitumen to a relationship between $|G^*|$ and frequency [58]. In Dickerson and Witt's paper, the relationship developed made use of the slope (or derivative) of the log-log relationship between the $|G^*|$ and frequency to estimate the phase angle. Christensen and Anderson (1992) further developed this by presenting a relationship between phase angle with frequency and binder fitting parameters that are needed to construct the full binder mastercurve [59]. Ma et al. (2011) introduced a new testing procedure to estimate the low-temperature properties of the RAP binder without extraction or chemical treatments. The testing procedure uses the Superpave® bending beam rheometer (BBR) with minor modification. The proposed

method has been verified and its capability of capturing the aged low-temperature properties of the binder in RAP materials has been confirmed [60].

For asphalt mixtures, several researchers have developed interrelationships between the phase angle and modulus. Bonnaure et al. (1977) developed a relationship that was limited to binder stiffness values greater than 5 MPa and less than 2 GPa [61]. During SHRP project Tayebali et al. (1994) developed a relationship linking the phase angle to the mix stiffness [62]. This relationship was developed from a study of fatigue properties. Christensen et al. (2003) published a relationship developed from the Hirsch model. This relationship links the phase angle to binder properties and mixture volumetric properties [63]. Zofka et al. (2005) evaluated the possibility of back-calculating the physical properties of the blended binders at the critical low temperature from the mixture stiffness determined in the Bending Beam Rheometer (BBR) using a modified Hirsch model [4]. Nam et al. (2010) evaluated the use of Hirsch model to backcalculate the properties of binder from some plant mixes containing RAP. For the binder used in this evaluation, the Hirsch model had the tendency to underestimate the binder $|G^*|$ at higher temperatures and the absolute back-calculation errors ranged from 0 to approximately 100 percent [5]. Also, Bennert et al. investigated the use of Hirsch model to back-calculate and determine the asphalt binder properties used in different mixtures. The proposed method correlates well with the measured data. However, general limitations exist where a dynamic modulus, $|E^*|$, of less than 30,000 psi will not provide accurate back-calculated $|G^*|$ values [64].

The need to know rheological characteristics of bituminous materials becomes more important when combined with the need to characterize the rheological properties of extracted binder from existing asphalt pavement. This need has increased with the use of more RAP into hot mix asphalt (HMA) to conserve resources and reduce costs. The extraction and recovery using solvents is a common method used to obtain binder to measure the properties of aged bitumen. However, the effect of solvents on the measured properties of recovered binders has been widely questioned in addition to the safety of the procedure. For estimation of the rheological properties of the existing binder, the binder from RAP mixtures needs to be extracted, tested and analyzed. During the construction and service life of the roadway, the asphalt binder ages which hardens the binder and changes the properties of binder before being used as RAP. Therefore, the properties of RAP materials need to be characterized properly to understand their characteristics at the time of construction. The aged binder from RAP is blended with the virgin binder in the mix design. This process affects the total binder grade and becomes more important when using a high amount of RAP in the mix design [65].

Therefore, a new approach to develop modeling techniques or use existing predictive models to back-calculate the rheological properties of binder from mixture properties would be useful for design and investigation of pavements. This would be of great interest if the predictions can cover a wide range of low, intermediate and high temperatures. Therefore, in this study two new predictive models were developed to determine the rheological properties of asphalt binder. It is believed that the proposed approach can lead to enhance the process of designing the HMA mixes with different RAP

contents without going through the challenging and destructive process of extraction and recovery.

4.2 Objective

This study was conducted to develop two new models which use the $|E^*|$ values of mixture, testing temperature, and few physical properties of mixtures. The models were developed using the time-temperature superposition principle and can be used to estimate the $|G^*|$ and phase angle of a binder for a wide range of needed testing conditions.

4.3 Theoretical Formulation

Traditionally, the $|G^*|$ of binder and $|E^*|$ of mixture are used to characterize the linear viscoelastic properties. The mechanical behavior of HMA mixtures is dominated by the viscoelastic nature of the asphalt binder. The specific characterization of asphalt concrete properties, such as the dynamic modulus, is based on the dependence of its behavior on both the time of loading and temperature, which can be shifted and merged into a single smooth sigmoidal function. This time-temperature dependent characterization of HMA mixtures reduces a three-dimensional problem to a two-dimensional problem by constructing a single mastercurve at a reference temperature. This simplification process can be done by utilizing the *time-Temperature Superposition* (*t-TS*) principle. It should be mentioned that, the subscript "$_M$" and "$_B$" refer to mixture and binder, respectively. The following sigmoidal function, Equation(19), can be used for this purpose.

$$\log|E^*| = a + \frac{b}{1+\frac{1}{e^{d+g\log(f_R^M)}}} \tag{19}$$

where,

$|E^*|$ = dynamic modulus, psi,

a = first sigmoidal coefficient; lower asymptote of $|E^*|$ mastercurve,

b = second sigmoidal coefficient, where $a+b$: refers to the high asymptote of $|E^*|$ mastercurve

d, g = parameters describing the shape of the sigmoidal function, and

f_R^M = reduced frequency of mixture at the reference temperature, *Hz*

The effects of time/frequency and temperature can be considered together in a single parameter referred to as *reduced time* or *reduced frequency*. These parameters can be combined by using the t-T shift factor defined in Equation(21).

$$f_R^M = f.a_T^M \tag{20}$$

$$\log(a_T) = \alpha_1 T^2 + \alpha_2 T + \alpha_3 \tag{21}$$

where,

$$\alpha_3 = -\alpha_1 T_R^2 - \alpha_2 T_R \tag{22}$$

and;

a_T = shift factor,

$\alpha_1,\ \alpha_2,\ \alpha_3$ = polynomial coefficients,

f = frequency of loading,

f_R = reduced frequency of loading at reference temperature,

T = temperature of interest

T_R = reference temperature (20 ºC was used in this study)

Also, the binder mastercurves can be constructed using a full suite of dynamic shear rheometer (DSR) test results measured at different testing conditions. Significant literature is available on using this type of equation (*2, 4, and 7*). In this study, Equation (23) is used for the binder mastercurve, and Equation (25) is used for the t-T shift factor concept. Equation (23) is known as the *Christensen-Anderson-Marasteanu* (CAM) model (*16*), and Equation (25) is a combination of the well-known *Williams-Landel-Ferry* (WLF) and *Arrhenius* models. A part of this model, Equation(25), recommended for temperatures greater than zero was used for the purpose of processing the binder |G*| test results and constructing the binder mastercurve in this study.

$$|G^*| = \frac{G_g}{\left(1+\left(\frac{f_c}{f_R^B}\right)^k\right)^{\frac{m_e}{k}}} = \frac{10^g}{\left(1+\left(\frac{f_c}{f_R^B}\right)^k\right)^{\frac{m_e}{k}}} \tag{23}$$

$$f_R^B = f.a_T^B \tag{24}$$

$$\log a_T^B = \begin{cases} \dfrac{E_a}{2.303\times R}\left(\dfrac{1}{273+T}-\dfrac{1}{273}\right)+\dfrac{C_1-T_R}{C_2-T_R} & \text{T} \le 0 \\ \dfrac{C_1\left(T-T_R\right)}{C_2+T-T_R} & \text{T} > 0 \end{cases} \tag{25}$$

where,

$|G^*|$ = dynamic shear modulus,

G_g = maximum shear modulus, glassy modulus (10^9 Pa),

T = test target temperature (°C),

T_R = reference temperature (20 °C),

R = gas constant (8.314 $J.K^{-1}.mol^{-1}$),

E_a = activation energy, determined through optimization (J/mol),

f_R = reduced frequency (Hz), and

f_c, m_e, k, C_1 and C_2 = fitting coefficients.

A reference temperature of 20°C is assumed for finding the shift factors of all mixtures and binders. It is possible to calculate the modulus values at any desired testing conditions (e.g., specific temperature and frequency) in question by using an optimization process and finding the functions in Equations (23), and (25). The formulation of the new binder predictive model is based on combining the mixture and binder master curves. For developing this model the mixture master curve is solved for reduced frequency of the mixture, which includes the temperature and frequency of testing. The subscripts "$_M$" and "$_B$" will be used for identifying mixture and binder characteristics. The formulation for the mixture reduced frequency is presented in Equation(26).

$$f_R^M = \left[e^d \times \left\{ \frac{b}{Log\,|E^*| - a} - 1 \right\} \right]^{\frac{-Ln10}{g}} \tag{26}$$

Using the same reference temperature, the amount of shift at each temperature will be different for the mixture and the binder. Therefore, a correction factor, presented in Equation(27), was used to consider this slight difference and was assumed as the ratio of the binder shift factor to mixture shift factor. The key point for relating the mixture and binder came from this equation. The reduced frequency of binder for constructing binder mastercurve was related to mixture properties through reduced frequency of mixture and

this correction factor. So, the correction factor would be a function of testing temperature and was found by fitting the best polynomial curve to both binder and mixture shift factors as illustrated in Equation(27). The average shift factors from all the calibration data points for binders and mixtures are used to determine the correction factor. This process has been further simplified by replacing Equation (21) and (22) in Equation(27).

$$\eta = \frac{a_T^B}{a_T^M} = \frac{f_R^B}{f_R^M} = \frac{10^{\alpha_{1B}(T^2 - T_R^2) + \alpha_{2B}(T - T_R)}}{10^{\alpha_{1M}(T^2 - T_R^2) + \alpha_{2M}(T - T_R)}} \tag{27}$$

For using the CAM model the reduced frequency of binder was needed which was derived by Equation(28).

$$f_R^B = \eta \times f_R^M \tag{28}$$

The combined CAM model and the reduced frequency of binder which is a function of mixture properties are the basis of developing the "|*G**| *model*", and is presented in Equation(29).

$$|G^*| = \frac{G_g}{\left(1 + \left(\frac{f_c}{(f_R^B)}\right)^k\right)^{\frac{m_e}{k}}} \tag{29}$$

where,

$$f_R^B = \eta \times \left[e^d \left\{ \frac{b}{Log\,|E^*| - a} - 1 \right\} \right]^{\frac{-Ln10}{g}} \tag{30}$$

The CAM model for estimating the phase angle, Equation(31), is also dependent on the reduced frequency of binder. In this case, the same expression for binder reduced frequency, Equation(30), was replaced to determine the relationship between the phase

angle of the binder, δ, and mixture properties. This relationship was used to develop the "*Phase Angle Model*" and is presented in Equation(31).

$$\delta = \frac{90m_e}{1+\left(\frac{f_R^B}{f_c}\right)^k} \tag{31}$$

Therefore, the combined relationships presented in Equations (29) and (31) were used to generate the new closed-form models for estimating the shear modulus and phase angle of binder after replacing the appropriate physical and mechanical properties of mixtures in Equation (30). To do so, the gradation and volumetric properties of mixtures were used to parameterize the "*a*" and "*b*" asymptotes in the mixture master curve and the mixture $|E^*|$ values was used as the main predictor.

4.4 Database Used in This Study

Most of the database used to generate the new predictive models was assembled and processed during the LTPP project [54]. This database was expanded later by assembling more databases that were collected at North Carolina State University (NCSU). Now, the database includes 20,209 data points from 1,008 mixes tested under different aging conditions and includes both modified and unmodified binders measured based on two test protocols, i.e., the AMPT and TP-62 protocols. This expanded database is referred to here as the "*Master NCSU*" database and consists of the NCSU, processed Witczak, Federal Highway Administration (FHWA) Mobile Trailer, WRI and Citgo databases. The Master database was subdivided into two subsets of the database that are used for calibrating and testing the performance of the new developed models. A large portion of the database, including the ones tested at NCSU, covers a wide range of testing

conditions, and this portion includes test results and was used to develop the new models. The remaining 10% of the expanded NCSU database with other available datasets were used to verify the models. A summary of the calibration NCSU database is presented in Table 6. It should be noted that all of the mixture dynamic modulus and binder shear modulus test measurements obtained from the laboratory were processed and merged into a single mastercurve by using the sigmoidal function and the Christensen-Anderson-Marasteanu (CAM) model [66], respectively. In each case the fitted values were found for the specific testing conditions (temperature and frequency) of TP-62 test protocol. So, the "measured" term used for these two material properties refers to the fitted values obtained from the related mastercurves. The comprehensive details of all these introduced databases can be found elsewhere [67].

Table 6 Summary of |E^*| Data Available in NCSU Calibration Mixture Database

Binder Code	No. of Mix Var.	Total No. of Tests	Temp. (°C)	Frequency (Hz)	Aging Condition	
					STOA*	LTOA* or Field
ALF-CRTB-76	1	5	-10, 10, 35, 54	25, 10, 5, 1, 0.5, 0.1, 0.05, 0.01	5	
ALF-SBSLG-70	1	3			3	
ALF-Terpolymer-70	1	4			4	
Citgo-Wilmington-64	42	118			111	7
MRL AAD-1-58	4	11			3	8
AA-Inman-64	3	9			9	
Citgo-Wilmington -70	15	37			37	
AA-Salisbury-76	1	3			3	
El Paso-Charlotte-64	2	6			6	
El Paso-Apex-64	1	3			3	
AA-Salisbury-70	1	3			3	
Patriot-AA-Greensboro-70	1	12			12	
Citgo-Charlotte-70	1	3			3	
Citgo-Charlotte-64	1	3			3	
AA-Salisbury-64	1	3			3	
Total	75	223			208	15
$\rho_{3/4}$		maximum		25		
		minimum		0		
$\rho_{3/8}$		maximum		55		
		minimum		1		
ρ_{4}		maximum		67		
		minimum		14		
ρ_{200}		maximum		7.2		
		minimum		2		
V_a		maximum		11.8		
		minimum		1.8		
V_{beff}		maximum		14.2		
		minimum		6		
VMA		maximum		21.5		
		minimum		9.5		
VFA		maximum		82.6		
		minimum		45.1		

* *STOA: Short term oven aging; LTOA: Long term oven aging*

$\rho_{¾}$, $\rho_{3/8}$, ρ_{4}, ρ_{200}: gradation parameters: percentage of cumulative retained on sieve size 3/4", 3/8" and #4 and passing sieve size #200 respectively, V_a (air void), V_{beff} (effective binder), VMA (volume of mineral aggregate) and VFA (voids filled with asphalt): volumetric properties of mixture are calculated based on the definitions in Superpave specification.

4.5 Modeling Approach

To develop the models, a set of dominant gradation and volumetric variables were identified to express the "*a*" and "*b*" terms which are the two asymptotes in the sigmoidal functions customarily used to create mixture mastercurve. The aforementioned process includes a series of the correlation, stepwise regression and principle component analysis that is discussed in detail elsewhere [67] due to the space limitation. In the next step, the coefficients used to express the binder mastercurve terms (f_c, m_e, k) and ones used in "*a*" and "*b*" terms were found simultaneously. This process was done by using the calibration database and through the Solver available in Excel. In the next step, "*a*" and "*b*" terms were found as a function of volumetric and gradation parameters. For both |*G**| and phase angle model, the "*a*" term will be a polynomial function of $\left(\rho_{3/4}, \rho_{3/8}, \rho_{200}, V_a, V_{beff}\right)$ and the "*b*" term will be a polynomial function of $\left(\rho_{200}, V_a, V_{beff}\right)$.The errors were optimized by comparing the measured |*G**| or phase angle with predicted |*G**| or phase angle values respectively. Then the sum of squared errors was minimized to find the best fitted coefficients in each case. It should be noted that the use of a nonlinear solver is recommended because of the nature of this problem and the number of variables that is needed to be found through the optimization process.

Also, an appropriate set of initial guesses was important to find the best fitted coefficients, which were found through the trial and error process. Both closed-form models were calibrated using the calibration data (90% of NCSU database). The remaining portion of master database was used for verification purpose. At the end, the best

predictive models were selected based on the best fitness statistics that were thoroughly assessed for both calibration and all sets of verification data. The selected "|*G**| *Model*" is presented in Equations(32)

$$|G^*| = \frac{145000}{\left(1+\left(\frac{0.2795}{X_B}\right)^{0.0959}\right)^{10.6879}} \tag{32}$$

where,

$$X_B = (10^{0.0004T^2-0.0135T-0.1003} \times \left[e^{0.972}\left\{\frac{\beta}{Log|E^*|-\alpha}-1\right\}\right]^{-7.591}) \tag{33}$$

$$\alpha = 5.633 - 0.00758\times\rho_{3/4} + 0.00346\times\rho_{3/8} + 0.08157\times\rho_{200} - 0.01721\times\rho_{200}^2 - 0.0908\times V_a - 0.37317\times V_{beff} + 0.01539\times V_{beff}^2 \tag{34}$$

$$\beta = 1.12 + 0.0233\times\rho_{200} + 0.00408\times\rho_{200}^2 + 0.0695\times V_a + 0.3849\times V_{beff} - 0.0169\times V_{beff}^2 \tag{35}$$

where,

$|G^*|$ = dynamic shear modulus (psi)

$|E^*|$ = dynamic modulus of mixture (psi)

T = test temperature (°C)

$\rho_{3/4}$ = cumulative percentage retained on the 3/4" sieve (19 mm), %

$\rho_{3/8}$ = cumulative percentage retained on the 3/8" sieve (9.5 mm), %

ρ_{200} = aggregate passing the #200 sieve (0.075mm), %

V_a = air voids (by V_{mix}), %

V_{beff} = effective asphalt content (by V_{total}), %

The same modeling approach was utilized to develop the phase angle model. The selected "*Phase Angle model*" is presented in Equation(36)

$$\delta = \frac{90 \times 1.044}{1 + \left(\frac{Y_B}{0.289} \right)^{0.1426}} \tag{36}$$

where,

$$Y_B = 10^{0.0004T^2 - 0.0135T - 0.1003} \times \left[e^{1.4199} \left\{ \frac{\gamma}{Log \mid E^* \mid - \lambda} - 1 \right\} \right]^{-8.334} \tag{37}$$

$$\lambda = 5.945 - 0.00151 \times \rho_{3/4} + 0.00099 \times \rho_{3/8} + 0.01861 \times \rho_{200} - 0.00891 \times \rho_{200}^2 - 0.0935 \times V_a - 0.4141 \times V_{beff} + 0.015064 \times V_{beff}^2 \tag{38}$$

$$\gamma = 1.1487 + 0.0209 \times \rho_{200} + 0.00523 \times \rho_{200}^2 + 0.059447 \times V_a + 0.4128 \times V_{beff} - 0.0158 \times V_{beff}^2 \tag{39}$$

where,

δ = phase angle (degree).

4.6 Performance of New Predictive Models

The new predictive models can be used to estimate the rheological properties of binders for a wide range of testing conditions which includes the critical very low and high temperature (e.g., -10 to 54.4 ºC) zones. The performance of these models was assessed on few independent verification datasets, which include some of the critical testing conditions as well as the test measurements from both the TP-62 test protocol (e.g., Witczak and 10% NCSU databases) and the AMPT test protocol (e.g., FHWA Mobile Trailer, WRI and Citgo databases). The performance of |*G**| model are shown in Figure 21(a) using calibration database (90% NCSU database) and Figure 21(b), (c) and (d) using 10% NCSU, Witczak and AMPT databases, respectively. The predicted versus measured values in these figures are presented align the line of equality (LOE) to show the bias and error terms that are presented in the right corner of plots more clearly.

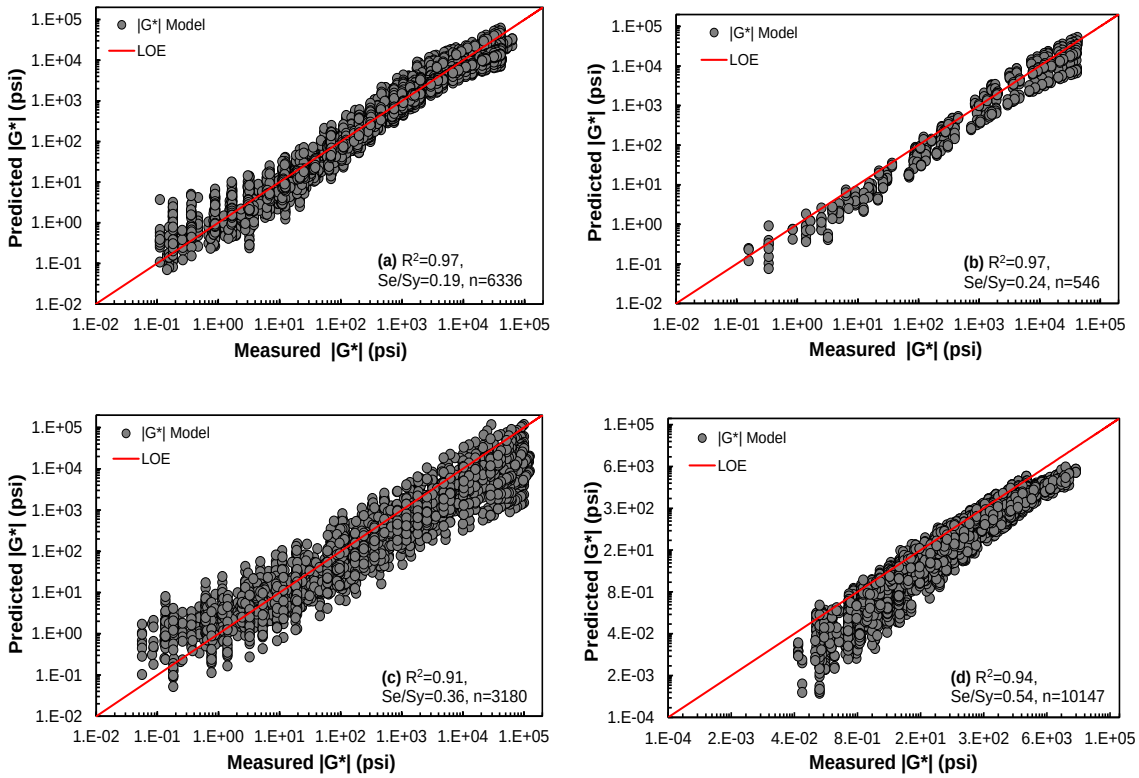

Figure 21 The |*G| Model Predictions Versus Measured Values Using (a) 90% NCSU, (b) 10% NCSU , (c) Witczak, and (d) AMPT Databases in Logarithmic Scale.**

The performance of phase angle models are shown in Figure 22 (a) using calibration database (90% NCSU database) and Figure 22 (b), (c) and (d) using 10% NCSU, Witczak and AMPT databases, respectively.

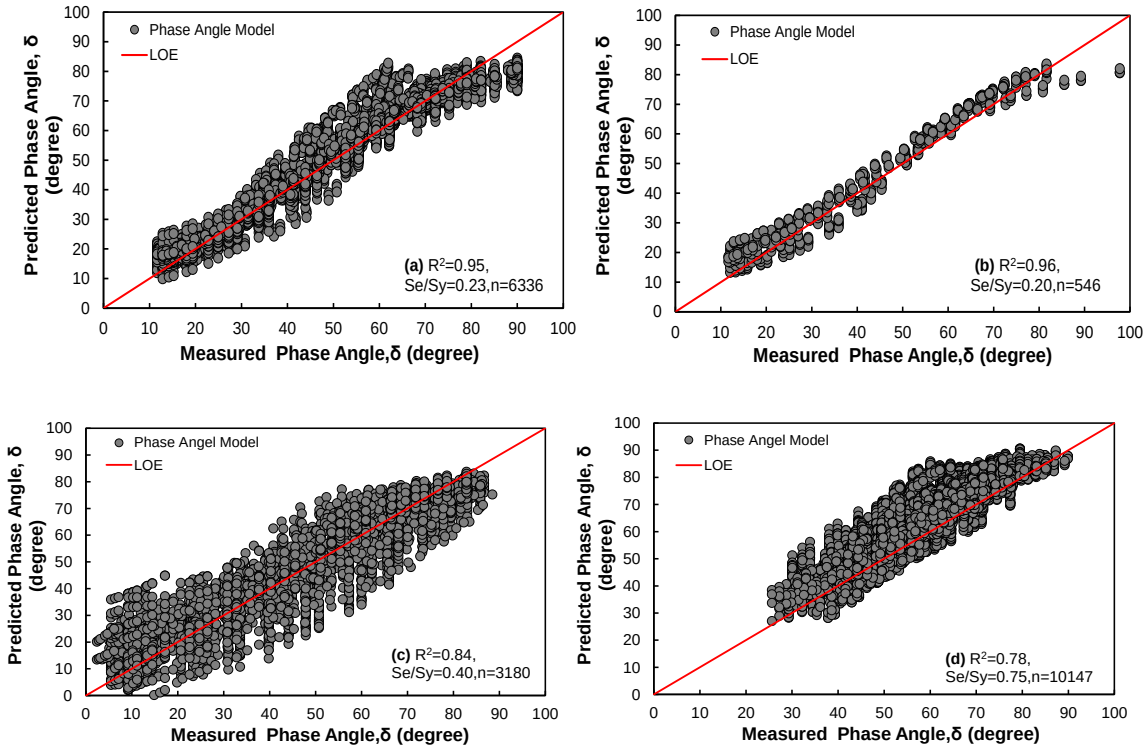

Figure 22 The Phase Angle Model Predictions Versus Measured Values Using (a) 90% NCSU, (b) 10% NCSU, (c) Witczak, and (d) AMPT Databases in Arithmetic Scale.

The error (Se/Sy) and bias (correlation coefficient, R^2) terms calculated for $|G^*|$ and phase angle models indicate a good fitness with relatively high correlation coefficients and low values of error for both verification and calibration databases as shown in Figure 21 and Figure 22. In general, the proposed models predict the modulus values and phase angles with a reasonable level of accuracy for all the investigated data sets. Further assessment of the performance of new developed models was done using a set of mixtures with a variety of different related binders having various performance grading. The

mixture with PG 64-28 binder from AMPT database and 6.76% mix air void, PG 64-22 from 10% NCSU database and 3.5% mix air void, PG 76-16 from Witczak database and 6.7% mix air void and PG 70-22 from 10% NCSU database with 3.9% mix air void were evaluated. Different types of mixtures and binders having various performance grading were chosen to evaluate the performance of new models. The binder mastercurve was then created using the predicted |*G**| and phase angle values and are compared against the measured values for mixtures from different databases in Figure 23I & II(a) and I and II(b). The results show that the new models can be used to estimate the rheological properties of binders by having the desired physical and mechanical properties of mixture with an acceptable level of accuracy. Further analyses were conducted to compare the back-calculated binder |*G**| with the corresponding measured values. The percent error of the back-calculation was determined using Equation(40).

$$\%\text{Error} = \frac{\text{Measured}\,|G^*| - \text{Predicted}\,|G^*|}{\text{Measured}\,|G^*|} \times 100 \tag{40}$$

The average percent errors for different mixtures are presented in the following. The absolute errors ranged from approximately 4% for phase angle predictions using mixture with PG 76-16 binder to 19.5% error for |*G**| predictions using a mixture with PG 64-22 binder.

- PG 64-28, form AMPT data; 15.05% error for |*G**| and 8.40% error for phase angle
- PG 64-22, form 10% NCSU data; 19.50% error for |*G**| and 13.60% error for phase angle
- PG 76-16, form Witczak data; 13.40% error for |*G**| and 4.14% error for phase angle
- PG 70-22, form 10% NCSU data; 13.57% error for |*G**| and 7.91% error for phase angle

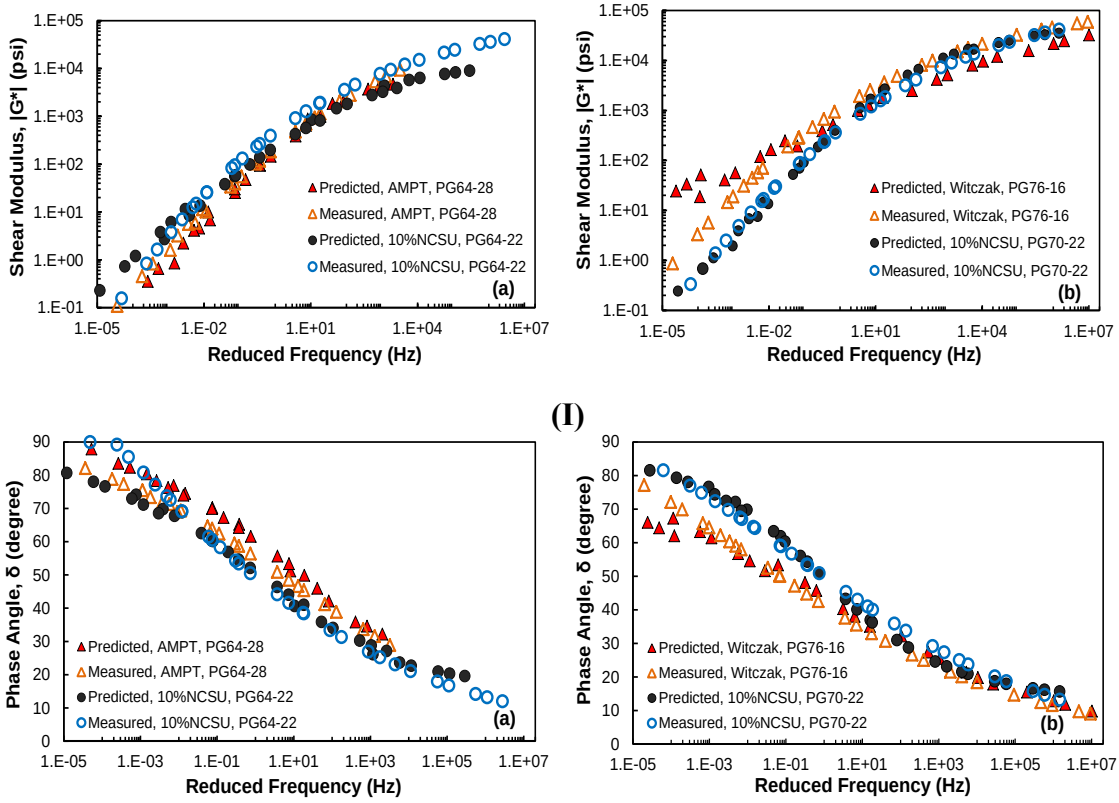

Figure 23 Predicted and Measured (I) Shear Modulus and (II) Phase Angle Mastercurves for (a) PG 64-28 from AMPT, PG 64-22, and (b), RAP in Mixtures

4.7 Performance of Existing Predictive Models (Hirsch Model)

Christensen et al. [63] examined four different models based on the law of mixtures and chose the model that incorporates the binder modulus and volumetric properties (VMA and VFA) because it provides accurate results in the simplest form. The other, more complicated forms attempt to incorporate the modulus of the mastic or the film thickness, which are difficult parameters to measure. The suggested model for the $|E^*|$ estimation is as follows:

$$|E^*|_m = P_c\left[4,200,000\left(1-\frac{VMA}{100}\right)+3|G^*|_b\left(\frac{VFA*VMA}{10,000}\right)\right]+\frac{(1-P_c)}{\frac{\left(1-VMA/100\right)}{4,200,000}+\frac{VMA}{3|G^*|_b\,(VFA)}}$$

(41)

$$\phi = -21(\log P_C)^2 - 55\log P_C \tag{42}$$

$$P_c = \frac{\left(20+3|G^*|_b\,(VFA)/(VMA)\right)^{0.58}}{650+\left(3|G^*|_b\,(VFA)/(VMA)\right)^{0.58}} \tag{43}$$

where,

$|E^*|_m$ = dynamic modulus of HMA in psi;

Pc = the aggregate contact volume;

VMA = percentage of voids in mineral aggregate in compacted mixture;

VFA = percentage of voids filled with asphalt in compacted mixture; and

ϕ = phase angle of HMA mixture.

A strength of this model is the *empirical phase angle equation for mixture*, which is important for the inter conversion of the $|E^*|$ to the relaxation modulus or creep compliance. It should be emphasized that the referred model can only be used for estimating the phase angle of mixture and not the asphalt binder. Weaknesses of the model include the lack of a strong dependence on volumetric parameters, particularly at low air void and VFA conditions. Also, questions arise regarding the ability of the $|G^*|_b$ parameter to account for the possible beneficial effects of modifiers [54]. Also, it must be noted that only 206 data points sampled from the FHWA-ALF, MnROAD and WesTrack experiments were used in determining the coefficients in the Hirsch model, compared to 2750 data points for the original Witczak model and 7400 data points for the modified Witczak model developed in NCHRP 1-40 [54].

A similar procedure for predicting the asphalt binder properties is discussed by Bennert et al. and Tran et al. [5, 64]. Therefore, the recommended procedure was adopted for further investigation in this study. The findings of these studies show that in spite of few limitations, the Hirsch model can be used for the back calculation of |*G**| values if the critical zones of very high or low temperatures that were not originally considered in the model development are not used. Due to these limitations, the predicted binder |*G**| values are not very accurate if |*E**| values less than 30,000 psi are used. Also, to be consistent with the newly developed models, the high values of |*G**| are limited to 1 GPa (145000 psi). These limitations led to reduced number of data points for comparing the performance of Hirsch and new developed models.

Therefore, the Hirsch model shown in Equation (41) was used to back-calculate the |*G**| of the binder from the mixture volumetric properties and |*E**| value. This back-calculation process was done by running an optimization code using MATLAB. Then, a mastercurve was created using the back-calculated |*G**| values from the Hirsch model by fitting the CAM model parameters. The fitted parameters were then used to calculate the phase angle values at the same testing conditions. The comparison between the back-calculated and measured |*G**| values are shown in Figure 24(a) for calibration database and verification datasets in Figure 24(b), (c) and (d). The results show that the predictions from Hirsch model are more accurate for intermediate temperatures and less insensitive to the volumetric and gradation changes at the critical low and high predicted values. It should be mentioned that the low |*E**| values were ignored in this assessment due to the limitations of Hirsch model recommended by Bennert et al. and Nam et al. [5, 64].

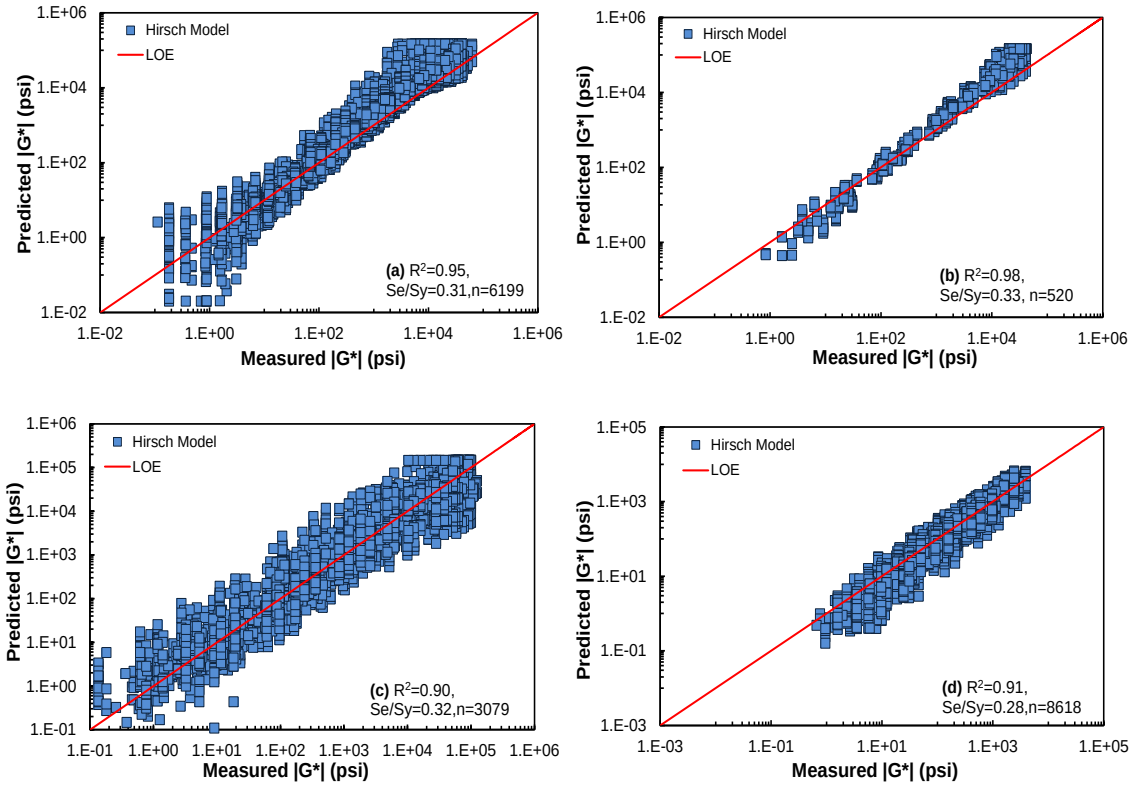

Figure 24 The Hirsch model |*G| Predictions Versus Measured Values for (a) 90% of NCSU, (b) 10% of NCSU, (c) Witczak, and (d) AMPT Databases in Logarithmic Scale.**

The phase angle predictions and statistic error and bias terms for each data base are shown in Figure 25. Figure 25(d) shows that the predicted phase angles for AMPT database have the tendency to be overestimated for the high values of phase angles. This observation is probably due to the fact that the Hirsch model was calibrated based on the |*E**| data measured using the laboratory prepared mixtures. Therefore, some back-calculation errors may be influenced by the difference between the laboratory prepared

and some of the plant produced HMA mixtures available in AMPT database. The overall evaluation of investigated data sets considering the important fact that the critical very low and high temperatures were ignored; show that Hirsch model can be used to predict the phase angle and shear modulus of binder with a higher degree of accuracy for only intermediate temperatures and not the very low and high temperature zones.

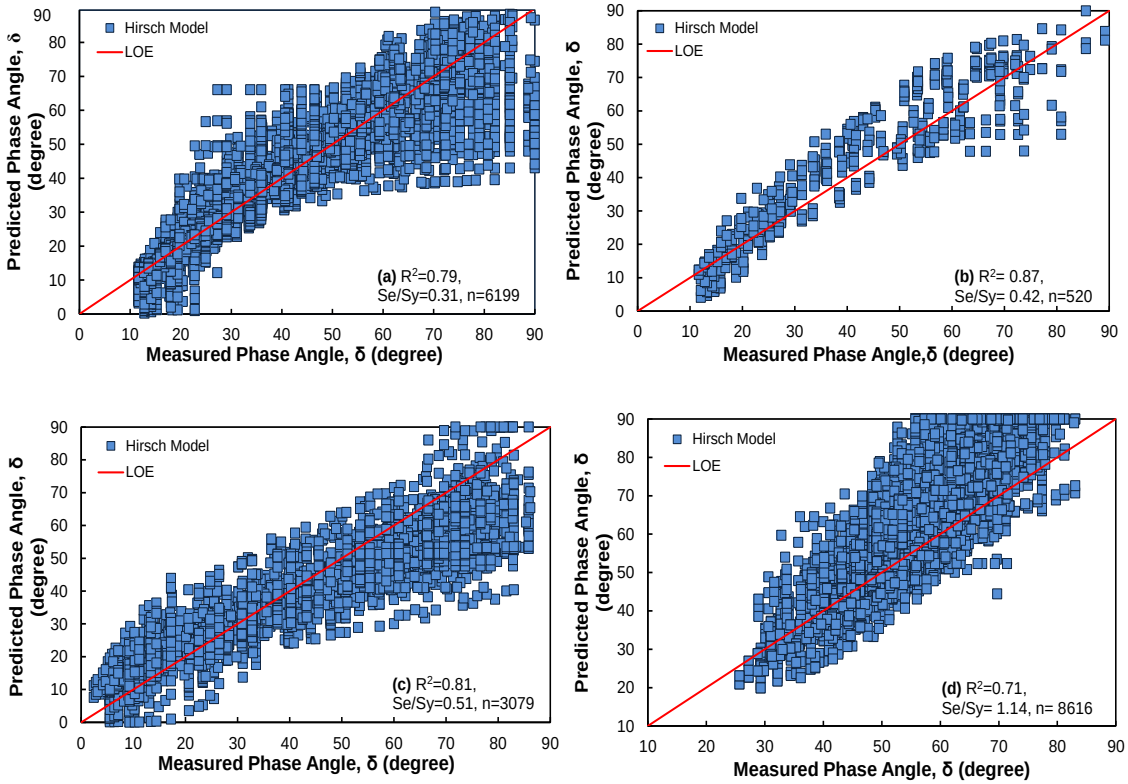

Figure 25 The Hirsch Model Phase Angle Predictions Versus Measured Values for (a) 90% of NCSU, (b) 10% of NCSU, (c) Witczak, and (d) APMT Databases in Arithmetic Scale.

Table 7 summarizes the correlation coefficient (R^2) and standard error terms for the new developed models and the Hirsch model for all verification and calibration data

sets. The shear modulus model was evaluated at the logarithmic scale and the statistics are in the referred scale, and the phase angle model was developed and evaluated in the arithmetic scale.

Table 7 Description of the Developed Models and their Statistics

Model	Reference Scale	Statistical Parameter for Calibration and Verification Data			
		90% NCSU	10% NCSU	Processed Witczak	AMPT
$\|G^*\|$ Model	Logarithmic	S_e/S_y= 0.19 R^2= 0.97 n^*= 6336	S_e/S_y= 0.22 R^2= 0.97 n= 546	S_e/S_y= 0.36 R^2= 0.91 n= 3180	S_e/S_y= 0.50 R^2= 0.94 n= 10147
Phase Angle Model	Arithmetic	S_e/S_y= 0.23 R^2= 0.95 n^*= 6336	S_e/S_y= 0.20 R^2= 0.96 n= 546	S_e/S_y= 0.40 R^2= 0.84 n= 3180	S_e/S_y= 0.72 R^2= 0.78 n= 10147
Hirsch (backcalculated $\|G^*\|$)	Logarithmic	S_e/S_y= 0.31 R^2= 0.95 n^*= 6199	S_e/S_y= 0.33 R^2= 0.98 n= 520	S_e/S_y= 0.32 R^2= 0.90 n= 3079	S_e/S_y= 0.28 R^2= 0.91 n= 8618
Hirsch (backcalculated phase angle)	Arithmetic	S_e/S_y= 0.31 R^2= 0.79 n^*= 6199	S_e/S_y= 0.42 R^2= 0.87 n= 520	S_e/S_y= 0.51 R^2= 0.81 n= 3079	S_e/S_y= 1.02 R^2= 0.71 n= 8616

** n=number of data points used for calculation of statistical parameters*

4.8 Summary and Recommendations for Future Study

A new modeling technique was presented that uses the mixture and binder mastercurves to determine the rheological properties of asphalt binders. As a result, two new models were developed that represent a complex case of characterizing viscoelastic materials by making the most use of available modeling techniques. These models can be applied for a wide range of needed testing conditions, including -10°, 4.4 °, 21.1°, 37.8° and 54.4 °C, which are the recommended testing conditions in AASHTO TP62-03 test

protocol. The new closed form models can be used to determine the rheological properties of binder. Having those properties predicted rather than measured through the process of extraction and recovery can lead to shorten the process of assessing the impact of RAP binders by utilizing one of the key inputs ($|E^*|$) needed in the MEPDG. The developed modeling techniques extend the use of previous research effort [54] that was conducted to convert the resilient modulus to $|E^*|$ values of HMA mixtures. Now, by using the procedures presented here one can convert the resilient modulus values of a mixture to the rheological properties of asphalt binder without running the dynamic modulus test.

This research study also presents an evaluation of two procedures for back-calculating the binder properties for a possible use in the RAP mix design process. However, it should be mentioned that to determine the binder critical high temperature, one needs to determine both the unaged and RTFO aged binder properties. The current Hirsch model and the newly developed models in this study were calibrated using the $|G^*|$ data determined using the RTFO aged binders. So it is recommended that to back-calculate the unaged binder physical properties, these models be calibrated using a new data set. However, another possibility would be to determine the binder critical high temperature for the RAP mix design solely based on the RTFO aged binder properties. Considering the variability of the RAP materials throughout the US, this option may be reasonable.

5. CONCLUSION AND RECOMMENDATIONS FOR FUTURE RESEARCH

Firstly, the chemistry and micro-rheology of the asphalt binder impact its macroscopic properties. The microstructures within two recovery methods were identified and characterized to investigate two different evaporate recovery methods that would be suitable to all emulsions. This study implemented a mechanical approach to investigating the impact that two different evaporative recovery methods have on microstructural and nano-rheological properties. The application of AFM as an imaging tool and extraction of nano-scale properties were implemented as inputs for modeling of microstructure of the binder. The conclusions from this study can be summarized as microstructural changes induced by different recovery methods, different mechanical properties of phases, different bulk behavior for different recovery procedures, and validation of behavior with simulation modeling.

The second goal of this research was to evaluate a mathematical model for characterizing asphalt without directly testing recovered binder. Two models were developed for prediction of binder rheological properties based on gradation and volumetric of the mixture. The new closed form models can be used to determine the rheological properties of binder. Having those properties predicted rather than measured through the process of extraction and recovery can lead to shortening the process of assessing the impact of RAP binders by utilizing one of the key inputs ($|E^*|$) needed in the MEPDG.

5.1 Conclusions

Based on the results obtained from topography images, adhesion images, dissipated energies, phase distribution, and elastic modules, convincing observations are apparent: different residue recovery methods impact not only the material behavior of these microstructures, but also the shape, size and distribution of each recovered asphalt, and the effects of long term aging profoundly decreased the difference between different recovery methods and control binder.

The main findings in this part of the study include:

- The strain sweep and multiple stress creep and recovery testing procedures, and related assessment criteria shown in this study, produce results that are able to distinguish different evaporative recovery methods.
- The Young modulus of phase 1 was higher in original aging condition of control binder as well as residue-recovered procedures. The process of aging binder increased the Young modulus of all phases in the binder microstructure. Procedure A (48 hours recovery) had the lowest amount of increase in Young modulus between original and PAV aging condition.
- Asphalt chemical parameters have a measurable effect on the aging of asphalt that can be observed with FTIR to reveal the oxidization and aging. The area under the peak between 1650 and 1820 wavenumber (cm^{-1}) was measured to determine if the asphalt was oxidizing during the curing processes. The Carbonyl areas were 0.69, 0.79, and 0.81 for control binder, 6 hours recovery, and 48 hours recovery respectively.

- Oxidative aging contributes considerably to the difference between emulsion residue properties and unaged virgin materials. It was shown by investigating the carbonyl area of FTIR spectrum that oxidative aging happens during the recovery procedures. Also it is hypostasized that remaining difference of strain tolerance and percent strain recovery can be attributed to effects of emulsifier.
- Simulation of control binder, and residue-recovered binders demonstrated the difference in behavior of these microstructures under tensile loading. The result of the simulations showed that the highest strain occurs in phase 2 of microstructures that might be a possible location for damage.
- The framework of viscoelastic indentation analysis presented in this study is based on the method of functional equations, which was developed by Vandamme [39]. The principles were illustrated for a trapezoidal loading by a conical indenter on Kelvin-Voigt creep model. The relaxation modulus values extracted from indentation test results, which yield more practically significant information for modeling and predicting asphalt behavior.
- The interesting finding is that the viscosity of the dashpot, and the stiffness of the spring, parallel with dashpot, decrease with residue recovery procedures. This finding in addition to higher dissipated energy indicates the dominant effect of emulsifying process in the residues obtained based on two adopted evaporative recovery procedures.

In the second part of the study two set of accurate predictive models for estimating the shear modulus |G*| of binder are developed. The primary inputs that are used in these new models include gradation, volumetric, and dynamic modulus of mixture |E*|. These models are capable of estimating binder rheological properties at different temperatures, loading frequencies, gradations and volumetric.

The main findings in this part of the study include:

- These models are developed based on five different datasets: processed Witczak, FHWA Mobile Trailer, NCDOT, WRI, and Citgo. These datasets contain a total of 1008 mixtures, 20209 data points while consisting of binder shear modulus and mixture dynamic modulus.
- In this study the Hirsch model is evaluated and compared to new models. The findings of these studies show that in spite of few limitations, the Hirsch model can be used for the back calculation of |*G**| values if the critical zones of very high or low temperatures that were not originally considered in the model development are not used. Due to these limitations, the predicted binder |*G**| values for Hirsch model are not very accurate if |*E**| values less than 30,000 psi are used. The new models cover a wide range of temperatures and frequencies.
- As shown in this study, these new developed models can be used to predict the full mastercurve of the binder for different binder grading. The binder mastercurve can be used to evaluate the performance of the binder under different loading conditions and different temperatures.

- Statistical sets were calculated for each model and for each data set separately. The new predictive |G*| model have coefficient of determinations between 0.94 and 0.97, and Se/Sy varies from 0.19 to 0.5.The new phase angle model have a coefficient of determination between 0.78 and 0.96, and Se/Sy varies from 0.2 to 0.72.

5.2 Future Work

To continue the research effectively, some areas where continued study is needed include:

- Testing of additional evaporative recovery methods that were not included in this work. Specifically the vacuum oven test [68] that eliminates oxygen from the process that prevents oxidative aging. It is important to understand that despite promising findings and good correlations between DSR and nano-mechanical properties, the data set that was tested makes it difficult to make robust conclusions regarding the exact influence of the recovery methods.
- Testing of additional emulsions that were not included in this work will provide insight for different type of emulsion and effects of recovery methods on different emulsion types and sources.
- Investigating different levels of polymer modification to isolate some of the effects due to polymer and those due to asphalt at micro structure level. This leads to linkage of chemical and mechanical behavior of modification process.

- Investigating the effects of temperature on the asphalt microstructure, which provides mechanical responses at different temperature. Also investigation of the effects of temperature on phase structuring and phase distribution.
- Evaluating the use of focused ion beam (FIB) to ablate the material at nano/micro scale. Also investigating the new surface with atomic force microscopy to demonstrate the occurrence of phases at the inner volume because atomic force microscopy investigates the properties of material at the surface.
- Implementing scanning electron microscopy in environmental mode for gathering images at perpendicular surfaces to investigate different phase at bitumen media.

Such knowledge of microstructure and linkage between chemical and mechanical properties offer the potential for using AFM technology to monitor and investigate the properties at a smaller scale and modify the material at a smaller scale.

For the second part of the study, the developed modeling techniques extend the use of previous research effort [54] that was conducted to convert the resilient modulus to $|E^*|$ values of HMA mixtures. Now, by using the procedures presented here one can convert the resilient modulus values of a mixture to the rheological properties of asphalt binder without running the dynamic modulus test.

However, it should be mentioned that to determine the binder critical high temperature, one needs to determine both the unaged and RTFO aged binder properties. The current Hirsch model and the newly developed models in this study were calibrated using the $|G^*|$ data determined using the RTFO aged binders. So it is recommended that to back-calculate the unaged binder physical properties, these models be calibrated using

a new data set. However, another possibility would be to determine the binder critical high temperature for the RAP mix design solely based on the RTFO aged binder properties.

REFERENCES

1. Kandhal, R. and B. Kennedy, *Hot Mix Asphalt Materials, Mixture Design and Construction.* NAPA Education Foundation, Lanham, MD, 1996.

2. USDOT(2013), *National Transportation Statistics. Department of Transportation,* Bureau of Transportation Statistics,Washington, D.C. , 2013.

3. Poel, V. and C. Der, *A General System Describing the Visco-Elastic Properties of Bitumens and its Relation to Routine Test Data.* Journal of Applied Chemistry, 1954. 4(5): P. 221-236.

4. Zofka, A., M. Marasteanu, X. Li, T. Clyne, and J. McGraw, *Simple Method to Obtain Asphalt Binders Low Temperature Properties from Asphalt Mixtures Properties (With Discussion).* Journal of the Association of Asphalt Paving Technologists, 2005. 74, P.255-282.

5. Tran, N., A.J. Taylor, R.C. West, A. Kvasnak, and P. Turner. *Evaluation of Predictive Models for Determination of Binder Critical High Temperature from Mixture Properties*. Transportation Research Board 89th Annual Meeting ,Washington, D.C., January 2010.

6. Hanz, A., Z. Arega, and H.U. Bahia. *Rheological Evaluation of Emulsion Residues Recovered Using Newly Proposed Evaporative Techniques*.Transportation Research Board 88th Annual Meeting, Washington, D.C. , January 2009.

7. Hanz, A.J., Z.A. Arega, and H.U. Bahia, *Rheological Behavior of Emulsion Residues Produced by Evaporative Recovery Method.* Transportation Research Record: Journal of the Transportation Research Board, 2010. 2179(1): P. 102-108.

8. Farrar, M.J., S.L. Salmans, and J.-P. Planche. *Recovery and Laboratory Testing of Asphalt Emulsion Residue: Application of the Simple Aging Test (SAT) and 4mm DSR. Transportation Research Board 92nd Annual Meeting*, Washington, D.C., January 2013.

9. Allen, R.G., D.N. Little, A. Bhasin, and R.L. Lytton, *Identification of the Composite Relaxation Modulus of Asphalt Binder Using AFM Nanoindentation.* Journal of Materials in Civil Engineering, 2012. 25(4): p. 530-539.

10. Nahar, S., B. Dillingh, S. Erkens, A.J. Schmets, H. Fischer, A. Scarpas, and G. Schitter. *Is Atomic Force Microscopy Suited as Tool for Fast Screening of Bituminous Materials? Interlaboratory Comparison Study*. *Transportation Research Board 92nd Annual Meeting, Washington, D.C.* , January 2013.

11. Kadrmas, A., *Emulsified Asphalt Residue Recovery Procedures in the United States.* Transportation Research E-Circular, 2007(E-C122).

12. Kadrmas, A. *Using Dynamic Shear Rheometer and Multiple Stress Creep Recovery to Compare Emulsion Residue Recovery Methods*. Transportation Research Board 88th Annual Meeting, Washington,D.C., January 2009.

13. Waters, J.C., G. Bosma, and P. Herrington, *Residual Binder Extraction from Emulsions for Quality Assurance Testing,* New Zealand Transport Agency Research Report, 2008.

14. Petersen, J.C., *A Review of the Fundamentals of Asphalt Oxidation: Chemical, Physicochemical, Physical Property, and Durability Relationships.* Transportation Research E-Circular, 2009 (E-C140).

15. Corbett, L. *Relationship between Composition and Physical Properties of Asphalt*. Proceedings of the Association of Asphalt Paving Technologists,Vol. 39,P.481, February 1970.

16. Jemison, H., B. Burr, R. Davison, J. Bullin, and C. Glover, *Application and Use of the ATR, FT-IR Method to Asphalt Aging Studies.* Fuel Science & Technology International, 1992. 10(4-6): P. 795-808.

17. Griffin, R., W. Simpson, and T. Miles, *Influence of Composition of Paving Asphalt on Viscosity, Viscosity-Temperature Susceptibility, and Durability.* Journal of Chemical and Engineering Data, 1959. 4(4): P. 349-354.

18. D'Angelo, J., *Effect of Polymer-Asphalt Binder Compatibility and Cross-Link Density of 35 Non-Recoverable Compliance in the MSCR Test Method.* Southeast Asphalt User/ Producer Group, San Antonio,Texas, 2007.

19. Allen, R., *Structural Characterization of Micromechanical Properties of Asphalt Using Atomic Force Microscopy. Master of Science Thesis.* Civil Engineering, Texas A&M University, 2010.

20. Takamura, K. and C. Lubbers, *Comparison of Emulsion Residues Recovered by the Forced Airflow and RTFO Drying.* AEMA/ISSA Proceedings, 2000: P. 1-17.

21. Dybalski, J.N. *Cationic Surfactants in Asphalt Adhesion*. Association of Asphalt Paving Technologists Proceedings. 1982.

22. Khosla, N.P. *Effect of Emulsified Modifiers on the Characteristics of Recycled Mixtures*. Association of Asphalt Paving Technologists Proceedings. 1982.

23. Lau, C., K. Lunsford, C. Glover, R. Davison, and J. Bullin, *Reaction Rates and Hardening Susceptibilities as Determined from Pressure Oxygen Vessel Aging of Asphalts.* Transportation Research Record, 1992 (1342).

24. Loeber, L., O. Sutton, J. Morel, J.M. Valleton, and G. Muller, *New Direct Observations of Asphalts and Asphalt Binders by Scanning Electron Microscopy and Atomic Force Microscopy.* Journal of Microscopy, 1996. 182(1): P. 32-39.

25. Loeber, L., G. Muller, J. Morel, and O. Sutton, *Bitumen in Colloid Science: A Chemical, Structural and Rheological Approach.* Fuel 77(13), 1998. P. 1443-1450.

26. Pauli, A., J. Branthaver, R. Robertson, W. Grimes, and C. Eggleston, *Atomic Force Microscopy Investigation of SHRP Asphalts: Heavy Oil and Resid Compatibility and Stability.* Preprints-American Chemical Society. Division of Petroleum Chemistry, 2001. 46(2): P. 104-110.

27. Allen, R.G., D.N. Little, A. Bhasin, and C.J. Glover, *The Effects of Chemical Composition on Asphalt Microstructure and their Association to Pavement Performance.* International Journal of Pavement Engineering, 2014. 15(1): P. 9-22.

28. Masson, J.F., V. Leblond, and J. Margeson, *Bitumen Morphologies by Phase-Detection Atomic Force Microscopy.* Journal of Microscopy, 2006. 221(1): P. 17-29.

29. Jäger, A., R. Lackner, C. Eisenmenger-Sittner, and R. Blab, *Identification of Microstructural Components of Bitumen by Means of Atomic Force Microscopy (AFM).* PAMM, 2004. 4(1): P. 400-401.

30. Maher, A. , T.A. Bennert, *Evaluation of Poisson's Ratio for Use in the Mechanistic Empirical Pavement Design Guide (MEPDG)*, 2008.

31. Tabor, D., *The Hardness of Metals*. Vol. 10. Clarendon Press,Oxford,1951.

32. Cheng, Y.-T. and C.-M. Cheng, *Scaling, Dimensional Analysis, and Indentation Measurements.* Materials Science and Engineering: Reports, 2004. 44(4): P. 91-149.

33. Doerner, M.F. and W.D. Nix, *A Method for Interpreting the Data from Depth-Sensing Indentation Instruments.* Journal of Materials Research, 1986. 1(04): P. 601-609.

34. Oliver, W.C. and G.M. Pharr, *An Improved Technique for Determining Hardness and Elastic Modulus Using Load and Displacement Sensing Indentation Experiments.* Journal of Materials Research, 1992. **7**(06): P. 1564-1583.

35. Hertz, H., *On the Contact of Elastic Solids.* J. Reine Angew. Math, 1881. 92(156-171): P. 110.

36. Boussinesq, Joseph. *Application Des Potentiels à l'étude de L'équilibre et Du Mouvement Des Solides Élastiques: Principalement au Calcul Des Déformations et Des Pressions Que Produisent, Dans Ces Solides, Des Efforts Quelconques Exercés sur une Petite Partie de Leur Surface ou de Leur Intérieur: Mémoire Suivi de Notes Étendues sur Divers Points de Physique, Mathematique et d'Analyse*,Gauthier-Villars,1885.

37. Love, A., *Boussinesq's Problem for a Rigid Cone.* The Quarterly Journal of Mathematics, 1939(1): P. 161-175.

38. Sneddon, I.N., *The Relation Between Load and Penetration in the Axisymmetric Boussinesq Problem for a Punch of Arbitrary Profile.* International Journal of Engineering Science, 1965. 3(1): P. 47-57.

39. Vandamme, M. and F.-J. Ulm, *Viscoelastic Solutions for Conical Indentation.* International Journal of Solids and Structures, 2006. 43(10): P. 3142-3165.

40. Domke, J. and M. Radmacher, *Measuring the Elastic Properties of Thin Polymer Films with the Atomic Force Microscope.* Langmuir, 1998. 14(12): P. 3320-3325.

41. Raghavan, D., M. Vanlandingham, X. Gu, and T. Nguyen, *Characterization of Heterogeneous Regions in Polymer Systems Using Tapping Mode and Force Mode Atomic Force Microscopy.* Langmuir, 2000. 16(24): P. 9448-9459.

42. Reynaud, C., F. Sommer, C. Quet, N. El Bounia, and T.M. Duc, *Quantitative Determination of Young's Modulus on a Biphase Polymer System Using Atomic Force Microscopy.* Surface and Interface Analysis, 2000. 30(1): P. 185-189.

43. Mondal, P., S.P. Shah, and L.D. Marks, *Nanoscale Characterization of Cementitious Materials.* ACI Materials Journal, 2008. 105(2).

44. Davydov, D. and M. Jirásek, *Modeling of Nanoindentation by a Visco-Elastic Porous Model with Application to Cement Paste*, *Nanotechnology in Construction 3*2009, Springer. P. 187-192.

45. Vandamme, M., *The Nanogranular Origin of Concrete Creep: A Nanoindentation Investigation of Microstructure and Fundamental Properties of Calcium-Silicate-Hydrates*, 2008, Massachusetts Institute of Technology.

46. Moeller, G., *AFM Nanoindentation of Viscoelastic Materials with Large End-Radius Probes.* Journal of Polymer Science Part B: Polymer Physics, 2009. 47(16): P. 1573-1587.

47. Jones, C.A. and Z.C. Grasley, *Short-Term Creep of Cement Paste During Nanoindentation.* Cement and Concrete Composites, 2011. 33(1): p. 12-18.

48. Jäger, A., R. Lackner, and K. Stangl, *Microscale Characterization of Bitumen–Back-Analysis of Viscoelastic Properties by Means of Nanoindentation.* International Journal of Materials Research, 2007. 98(5): P. 404-413.

49. Binnig, G., C.F. Quate, and C. Gerber, *Atomic Force Microscope.* Physical Review Letters, 1986. 56(9): P. 930.

50. Lee, E.H. and J.R.M. Radok, *The Contact Problem for Viscoelastic Bodies.* Journal of Applied Mechanics, 1960. 27(3): P. 438-444.

51. Rasband, W., *ImageJ, US National Institutes of Health, Bethesda, Maryland, USA, 1997-2011.* There is no corresponding record for this reference, 2011.

52. Serry, F., *Improving the Accuracy of AFM Force Measurements: The Thermal Tune Solution to the Cantilever Spring Constant Problem.* Veeco Application Notes, 2005: P. 1-4.

53. New, O. and R. Pavement, *Guide for Mechanistic-Empirical Design.* 2003.

54. Kim, Y.R., B. Underwood, M.S. Far, N. Jackson, and J. Puccinelli, *LTPP Computed Parameter: Dynamic Modulus*, 2011.

55. Velankar, S. and D. Giles, *How Do I know If My Phase Angles Are Correct?* Rheology. Bull, 2007. 76(8).

56. Rowe, G. *Phase Angle Determination and Interrelationships within Bituminous Materials*. *Proceedings of the 7th International RILEM Symposium on Advanced Testing and Characterization of Bituminous Materials, Rhodes, Greece,(Book 1, Edited by Loizos, Partl, Scapas & Al-Qadi), May*. 2009.

57. Valdés, G., F. Pérez-Jiménez, R. Miró, A. Martínez, and R. Botella, *Experimental Study of Recycled Asphalt Mixtures with High Percentages of Reclaimed Asphalt Pavement (RAP).* Construction and Building Materials, 2011. 25(3): P. 1289-1297.

58. Dickinson, E. and H. Witt, *The Dynamic Shear Modulus of Paving Asphalts as a Function of Frequency.* Transactions of the Society of Rheology (1957-1977), 1974. 18(4): P. 591-606.

59. Christensen, D.W. and D.A. Anderson, *Interpretation of Dynamic Mechanical Test Data for Paving Grade Asphalt Cements (With Discussion).* Journal of the Association of Asphalt Paving Technologists, 1992. 61.

60. Ma, T., E. Mahmoud, and H.U. Bahia, *Estimation of Reclaimed Asphalt Pavement Binder Low-Temperature Properties Without Extraction.* Transportation Research Record: Journal of the Transportation Research Board, 2010. 2179(1): P. 58-65.

61. Bonnaure, F., G. Gest, A. Gravois, and P. Uge, *A New Method of Predicting the Stiffness of Asphalt Paving Mixtures*, Annual Meeting of the Association of Asphalt Paving Technologists, San Antonio, TX, February 1977.

62. Tayebali, A.A., J.A. Deacon, J.S. Coplantz, J.T. Harvey, and C.L. Monismith, *Mix and Mode-of-Loading Effects on Fatigue Response of Asphalt-Aggregate Mixes (With Discussion).* Journal of the Association of Asphalt Paving Technologists, 1994. 63.

63. Christensen Jr, D., T. Pellinen, and R. Bonaquist, *Hirsch Model for Estimating the Modulus of Asphalt Concrete.* Journal of the Association of Asphalt Paving Technologists, 2003. 72.

64. Bennert, T. and R. Dongré, *Backcalculation Method to Determine Effective Asphalt Binder Properties of Recycled Asphalt Pavement Mixtures.* Transportation Research Record: Journal of the Transportation Research Board, 2010. 2179(1): p. 75-84.

65. McDaniel, R.S., H. Soleymani, R.M. Anderson, P. Turner, and R. Peterson, *Recommended Use of Reclaimed Asphalt Pavement in the Superpave Mix Design Method.* NCHRP Web document, 2000. 30.

66. Zeng, M., H.U. Bahia, H. Zhai, M.R. Anderson, and P. Turner, *Rheological Modeling of Modified Asphalt Binders and Mixtures (With Discussion).* Journal of the Association of Asphalt Paving Technologists, 2001. 70.

67. Sakhaei Far, M.S., *Development of New Dynamic Modulus (: E*:) Predictive Models for Hot Mix Asphalt Mixtures*: North Carolina State University, 2011.

68. Kadrmas, A., *Asphalt Emulsion Residue Recovery Update.* Progress Toward Performance-Graded Emulsified Asphalt Specifications, 2013: P. 8.